[American Journal of Science, Vol. 313, May, 2013, P. 452–489, DOI 10.2475/05.2013.02]

PALEOREDOX AND PYRITIZATION OF SOFT-BODIED FOSSILS IN THE ORDOVICIAN FRANKFORT SHALE OF NEW YORK

ÚNA C. FARRELL*,**,†, DEREK E. G. BRIGGS*,***, EMMA U. HAMMARLUND§, ERIK A. SPERLING§§, and ROBERT R. GAINES§§§

ABSTRACT. Multiple beds in the Frankfort Shale (Upper Ordovician, New York State), including the original "Beecher's Trilobite Bed," yield fossils with pyritized soft-tissues. A bed-by-bed geochemical and sedimentological analysis was carried out to test previous models of soft-tissue pyritization by investigating environmental, depositional and diagenetic conditions in beds with and without soft-tissue preservation. Highly-reactive iron (Fe_{HR}), total iron (FeT), $\delta^{34}S$, organic carbon and redox-sensitive trace elements were measured. In particular, the partitioning of highly-reactive iron between iron-carbonates (Fe-carb), iron-oxides (Fe-ox), magnetite (Fe-mag), and pyrite (FeP) was examined.

Overall, the multi-proxy sedimentary geochemical data suggest that the succession containing pyritized trilobite beds was deposited under a dysoxic water-column, in agreement with the paleontological data. The data do not exclude brief episodes of water-column anoxia characterized by a ferruginous rather than an euxinic state. However, the highest Fe_{HR}/FeT values and redox-sensitive trace element enrichments occur in siltstone portions of turbidite beds and in concretions, suggesting that subsequent diagenesis had a significant effect on the distribution of redox-sensitive elements in this succession. Moderately high Fe_{HR}/FeT and FeP/Fe_{HR}, low organic carbon, enriched $\delta^{34}S$, and the frequent presence of iron-rich carbonate concretions in beds with soft tissue preservation confirm that pyritization was favored where porewaters were iron-dominated in sediments relatively poor in organic carbon.

Key words: Dysoxia, iron paleoredox proxy, Konservat Lagerstätte, taphonomy, trace elements, sulfur isotopes, distal turbidite, paleoenvironment

INTRODUCTION

Preservation of soft-tissues in pyrite is widespread in the Late Ordovician Lorraine Group of Upstate New York, where it occurs in multiple beds at the classic Beecher's Trilobite Bed (BTB) site in the Frankfort Shale, and at other localities in the Taconic Foreland Basin (Farrell and others, 2009, 2011). Previous studies determined the reactive iron content, sulfur isotopic composition of pyrite, organic carbon content, and pyrite framboid size and morphology through a section including the original Beecher's Trilobite Bed (OTB) and compared the results with the Devonian Hunsrück Slate, which also yields pyritized fossils. It was shown that pyritization of soft tissues requires rapid burial in anoxic sediment (to reduce bioturbation and place carcasses in the zone of sulfate reduction) with low organic carbon and high reactive iron content (to concentrate iron sulfide formation around decaying carcasses) (Briggs and others, 1991, 1996; Raiswell and others, 2008). Here, we use a multi-proxy geochemical

* Department of Geology and Geophysics, Yale University, P.O. Box 208109, New Haven, Connecticut 06520-8109, USA
** Biodiversity Institute, University of Kansas, Lawrence, Kansas 66045, USA; ufarrell@ku.edu
*** Yale Peabody Museum of Natural History, Yale University, New Haven, Connecticut 06520, USA; derek.briggs@yale.edu
§ Nordic Center for Earth Evolution and Institute of Biology, University of Southern Denmark, Odense C, Denmark; emma@biology.sdu.dk
§§ Department of Earth and Planetary Sciences, Harvard University, Cambridge, Massachusetts 02138, USA; sperling@fas.harvard.edu
§§§ Geology Department, Pomona College, Claremont, California 91711, USA; Robert.Gaines@pomona.edu
† Corresponding author: ufarrell@ku.edu

analysis to provide new insight into the diagenetic conditions that prevailed at the BTB site and, in conjunction with paleoecological data (Farrell and others, 2011), help to constrain the paleoenvironmental setting.

In particular, the discovery of multiple new beds with pyritized trilobites ("trilobite beds") allows us to determine whether the geochemical signatures in the OTB (iron enrichment and elevated $\delta^{34}S$ of bulk sediments: Briggs and others, 1991; Raiswell and others, 2008) are diagnostic of beds with soft-tissue pyritization or occur in other beds in the succession. Although the beds with pyritized soft tissues share similar lithological characteristics, the succession also includes a range of different bed types ranging from coarser siltstone turbidites to hemipelagic mudstones (Farrell and others, 2009, 2011; fig. 1). Furthermore, previous investigations have yielded different interpretations of the redox conditions under which pyritization of soft tissues occurred. Interpretations of water-column conditions during deposition of the Frankfort Shale have ranged from anoxic or occasionally anoxic (Hannigan and Mitchell, 1994; Lehmann and others, 1995), dysoxic/within an oxygen minimum zone (Cisne, 1973; Cisne and others, 1982; Hay and Cisne, 1988), to oxic (Briggs and others, 1991; Raiswell and others, 2008). The Frankfort Shale succession at the BTB site consists primarily of medium to dark gray mudstones with a low-diversity fauna and limited bioturbation, suggestive of dysoxic benthic conditions (Cisne, 1973; Briggs and others, 1991; Farrell and others, 2009, 2011). In association with the paleoecology (Farrell and others, 2011), the geochemical proxies allow us to gain a more comprehensive understanding of water-column conditions when the Frankfort shale was deposited.

The iron speciation method, which determines the nature of "highly-reactive" iron (that is, the distribution of iron phases that are reactive towards sulfide on a short timescale) in fine-grained sediments, has been used to examine both paleoenvironmental and taphonomic conditions in ancient settings (for example, Raiswell and others, 2001; Poulton and others, 2004; Canfield and others, 2007, 2008; Johnston and others, 2010; Boyer and others, 2011; Raiswell and others, 2011; Johnston and others, 2012). A range of studies have shown that under euxinic water-column conditions, enrichments in highly-reactive iron (Fe_{HR}) relative to total iron (FeT) are mainly a product of the formation of syngenetic pyrite in the water-column, whereas under anoxic and non-sulfidic conditions, enrichments in highly-reactive iron are mainly in the form of iron carbonates (Poulton and others, 2004; Poulton and Canfield, 2005; März and others, 2008; Johnston and others, 2010). A threshold of $Fe_{HR}/FeT > 0.38$ is used in many studies (for example, Canfield and others, 2008; März and others, 2008; Johnston and others, 2010) to identify anoxic water-column conditions, based on empirical measurements from modern oxic and anoxic settings (Raiswell and Canfield, 1998). However, because Fe-enrichment results in most cases from flux of highly-reactive Fe from the water-column to the sediments, the water-column signal may be altered or overwhelmed by episodic sedimentation (Coleman, 1985; Wilson and others, 1986; Bloch and Krouse, 1992; Mucci and Edenborn, 1992; Kasten and others, 1998; Anderson and Raiswell, 2004; Lyons and Severmann, 2006; Raiswell and others, 2008; Aller and others, 2010). Therefore understanding the depositional context is essential.

Redox-sensitive trace elements provide a means of determining water-column redox conditions independent of iron-based proxies (for example, Calvert and Pedersen, 1993; Wignall, 1994; Tribovillard and others, 2006; Algeo and Maynard, 2008). We examined a suite of nine redox-sensitive trace elements: Mo, U, V, Pb, Zn, Cu, Co, Cd, Ni, in addition to the minor element, Mn. Of these, Mo is considered one of the more reliable indicators of paleoredox conditions, especially euxinic conditions, due in part to its low concentration in the detrital fraction compared to its abundance as an authigenic component in reducing settings (for example, Calvert and Pedersen, 1993;

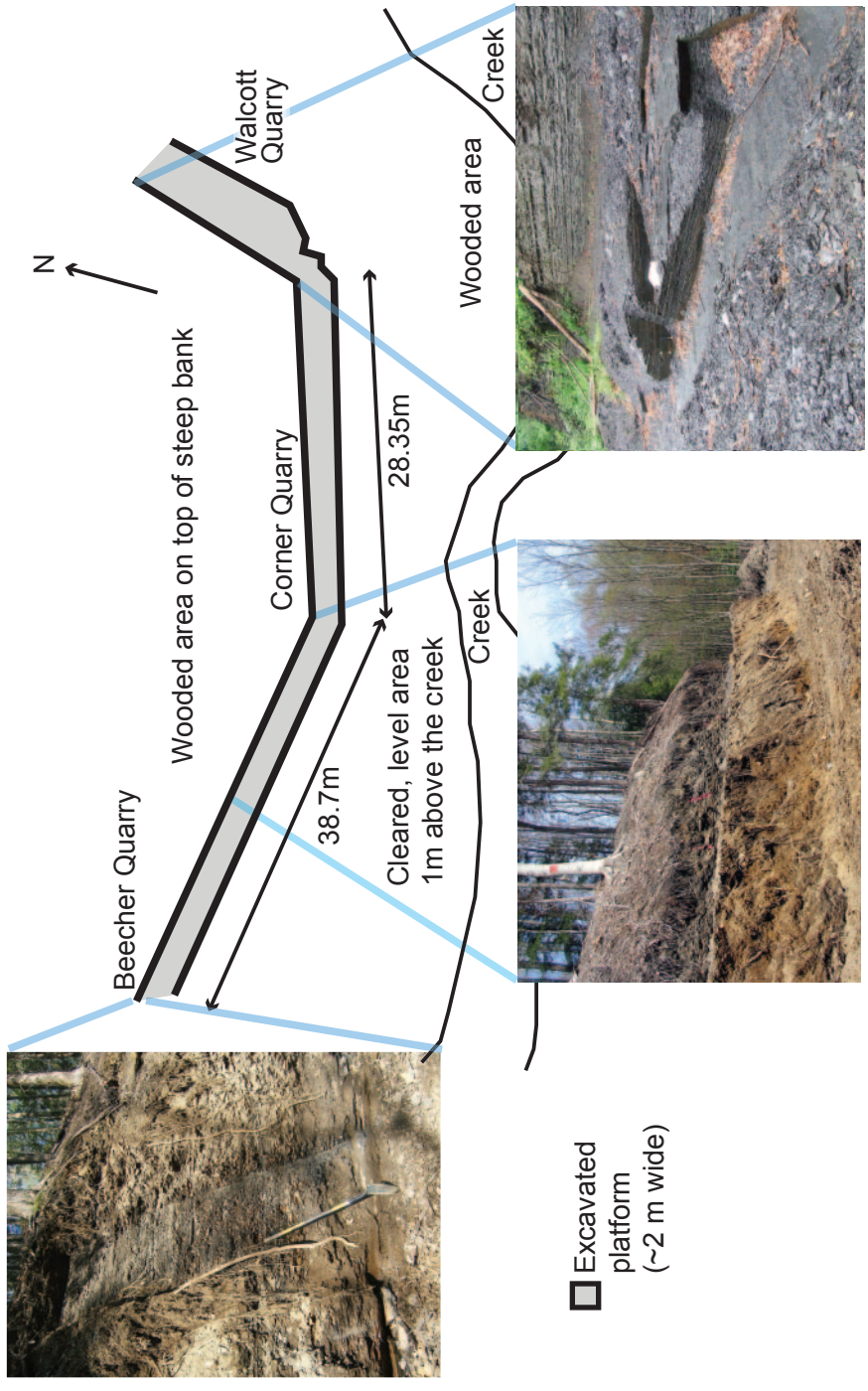

Fig. 1. Sketch map of the BTB site showing the location of the three logged sections: Beecher Quarry, Corner Quarry, and Walcott Quarry. The Walcott and Beecher Quarries were named for the paleontologists who worked there in the late 1800's. The Walcott Quarry was the site of a previous excavation in 1989 (Briggs and others, 1991, 1996). White data points = prominent siltstone layers (see text).

Crusius and others, 1996; Algeo and Lyons, 2006; Lyons and others, 2009; Xu and others, 2012a).

The isotopic signature of sulfur in pyrite ($\delta^{34}S$) is also examined, as it may reflect sulfate availability as well as rate of sulfate reduction in both water-column and sediments (for example, Jørgensen, 1979; Goldhaber and Kaplan, 1980; Habicht and Canfield, 2001). However, this biogeochemical tool is also influenced by factors such as sedimentation rate, sediment type, organic carbon content, depth of pyrite precipitation, and the extent of bioturbation (Bickert, 2006 and references therein) and interpretation is therefore dependent on a thorough understanding of the depositional context.

The geochemical data are also compared with paleoecological inferences of redox state (Savrda and Bottjer, 1991; Tyson and Pearson, 1991 and references therein; Droser and Bottjer, 1993; Wignall, 1993, 1994; Levin and others, 2000; Gaines and Droser, 2003). The low-diversity of bedding plane body fossil assemblages in the sections studied (representative of local water-column conditions), and the low-diameter and low-diversity burrows indicate that bottom water conditions were generally low in oxygen (Farrell and others, 2011). The benthic sessile fauna—predominantly small infaunal and epifaunal brachiopods and bivalves—were well adapted to low-oxygen conditions (Thompson and others, 1985; Levin, 2003; Boyer and Droser, 2009; Farrell and others, 2011). *Triarthrus,* a benthic deposit-feeder (Whittington and Almond, 1987) was also well adapted to low-oxygen conditions, with long respiratory filaments comparable to many modern dysoxic residents (Whittington and Almond, 1987; Levin and others, 2000; Farrell and others, 2011). Fortey (2000) suggested that *Triarthrus* may have been a chemoautotrophic symbiont tolerant of sulfur-rich conditions. However, the presence of *in situ* benthic organisms on essentially all bedding planes suggests that conditions were rarely, if ever, truly anoxic (Farrell and others, 2011). Bedding planes yielding abundant planktonic graptolites may represent an exception, but upon close examination, most of the graptolite-rich beds also reveal the presence of small benthic brachiopods (Farrell and others, 2009, 2011). The combined geochemical and paleontological inferences give new insights into the environmental and taphonomic conditions under which the exceptionally-preserved pyritized trilobites were preserved.

MATERIAL AND METHODS

Microstratigraphy and Sedimentology

Following extensive excavation, the fossil-bearing succession was logged at three positions across the exposed face of the outcrop: Beecher Quarry, Corner Quarry and Walcott Quarry (fig. 1; Farrell and others, 2009, 2011). Locality details are available from the Yale Peabody Museum upon request. The strata of the Frankfort Shale that crop out there are nearly flat-lying and individual beds could be correlated across the extent of the excavation. A continuous interval 110 cm in thickness was sampled at the Walcott Quarry and subjected to bed-by-bed sedimentological and geochemical analysis in order to determine the effect of fine-scale sedimentological heterogeneity on the geochemical signature (fig. 1). Additional bed-by-bed sampling was undertaken at the Beecher and Corner Quarries to determine variation along-strike (fig. 1). A representative selection of samples was prepared as thin-sections and polished slabs, and was x-radiographed for fine-scale examination of sedimentary structures and textures (Farrell and others, 2011).

Geochemical Analyses

Highly-reactive iron is operationally defined, and the techniques for determining reactive iron content have been refined a number of times (Berner, 1969; Canfield and

others, 1992; Raiswell and others, 1994; Raiswell and Canfield, 1998; Poulton and Canfield, 2005; Raiswell and others, 2011). We used the extraction method of Poulton and Canfield (2005), where highly-reactive iron (Fe_{HR}) is defined as pyrite iron (FeP) plus iron phases that react with sulfide on a short time scale (generally days to weeks), that is, iron associated with carbonates (Fe-carb), iron from oxides and oxyhydroxides (Fe-ox), and magnetite iron (Fe-mag). In this paper, operationally-defined pools (for example, Fe_{HR}) are denoted by a subscript whereas analytical values, such as total iron (FeT), are denoted by capitalized terms (Raiswell and Canfield, 1998).

In a series of sequential extractions to quantify different fractions of "highly reactive" iron, aliquots of powdered rock (grain size <63 μm) were first subjected to a 1M sodium acetate solution (acetic-acid buffered to pH 4.5), for 48 hours at 50 °C. Seven separate sets of replicate samples yielded standard deviations between 0.001 and 0.06. This solution extracts carbonate iron (Fe-carb), including crystalline siderite and ankerite, while leaving iron oxides/oxyhydroxides and iron bound in clay minerals minimally affected (Poulton and Canfield, 2005). Raiswell and others (2011) demonstrated that in some cases siderite iron is not quantitatively extracted by the acetate extraction, although this caveat might mainly apply to crystalline, extremely siderite-rich Banded Iron Formation such as in that study. Iron from oxides and oxyhydroxides (Fe-ox) was extracted subsequently by placing the same samples in a sodium dithionite solution (citric acid-buffered to pH 4.8) at room temperature for two hours. Replicate samples yielded standard deviations between 0.001 and 0.04. Finally, magnetite iron (Fe-mag) was extracted using an ammonium oxalate solution (pH = 3.2, oxalic acid-buffered) at room temperature for six hours. Replicate samples yielded standard deviations between 0.005 and 0.12. Atomic absorption flame spectroscopy (AAS) was used to measure the iron content of each extraction.

A subset of samples was further analyzed using the iron extraction method of Raiswell and Canfield (1998), which follows Canfield (1989) in using a 1-hour room temperature extraction in the sodium dithionite solution described above. After one hour, a small aliquot was removed for measurement, and the extraction was allowed to proceed for another hour for comparison with the results of the sequential extraction (Poulton and Canfield, 2005).

Pyrite content was determined using the chromous chloride reduction method (Zhabina and Volkov, 1978; Canfield and others, 1986). The method extracts and precipitates pyrite-sulfur as a silver sulfide. Subsequently, pyrite-iron (FeP) content is calculated using pyrite stoichiometry (assuming iron sulfide is present as FeS_2). Duplicates of four samples yielded differences between 0.01 percent and 0.08 percent. Reduced sulfur may occur in other minerals in sedimentary rocks, including iron monosulfides such as pyrrhotite and greigite, or potentially in copper- or zinc-sulfides if there has been hydrothermal fluid flow. If such minerals—collectively referred to as acid-volatile sulfides (AVS)—were present, the FeP content would be over-estimated. To test this possibility, a subset of samples was tested for the presence of AVS using the hot 6N HCl treatment of Rice and others (1993). Visual inspection of the silver sulfide traps revealed only trace amounts (below the gravimetric quantification limit of ~0.001 wt %) in three of the samples while the rest showed none; based on this subset AVS does not appear to exist in appreciable quantities in these rocks.

The sulfur isotopic composition of pyrite was determined using the silver sulfide precipitate described above. Between 0.4 and 0.8 mg of silver sulfide was weighed into aluminum cups. Around 2 mg of vanadium pentoxide were added (actual mass noted) and the cups were folded into pellets. The samples were analyzed by combustion at Iso-Analytical labs, England. Three sets of replicates of standards from Iso-analytical labs had standard deviations between 0.04 and 0.14 permil. Four sets of duplicate samples exhibited a percent difference between 0.00 percent and 0.04 percent. Two

samples (from beds 822 and 906) were measured from whole rock powders (based on the assumption that all sulfur in the sediment was present as pyrite). Around 10 mg powdered sediment and 10 mg tungsten oxide (WO_3) were weighed into aluminum cups. These samples were analyzed by combustion at the Earth Systems Center for Stable Isotopic Studies at Yale University.

Inorganic and organic carbon contents were measured by SGS Labs, Canada, using infrared (IR) spectroscopy of CO_2 liberated from powdered whole rock samples. Inorganic carbon was measured in a second batch of powdered whole rock samples using CO_2 coulometry at Pomona College. A multi-acid digestion (hydrofluoric, perchloric, hydrochloric, and nitric) was used to extract total iron (FeT), aluminum, sulfur and trace elements at SGS and Acme labs in Canada. Trace elements Mo, U, V, Pb, Zn, Cu, Co, Cd, Ni and the minor element Mn were measured using ICP-AES or ICP-MS. Trace element data were normalized to Al, on the assumption that Al occurs entirely in the aluminosilicate phase in fine-grained siliciclastic sediments and provides a reliable proxy for the detrital fraction (Calvert and Pedersen, 1993; Dean and others, 1997; Algeo and others, 2004). Four sets of duplicate samples from ACME labs and four sets of duplicates from SGS were run for each major, minor and trace element analyzed and yielded a percent difference of between 0 and 0.3 percent, with a mean percent difference of 0.03 percent. Higher percent differences were noted where concentrations were close to the detection limit (in particular, Cd). One sample (concretion from bed 1004) was analyzed subsequently by XRF at Pomona College using a fused glass bead prepared following the method of Johnson and others (1999). Enrichment factors (EF) were used to compare trace element concentrations (X) to those in average shale (WSA, that is "world shale average": Turekian and Wedepohl, 1961; Wedepohl, 1971): $EF_{\text{trace element}} = (X/Al)_{\text{sample}}/(X/Al)_{\text{average shale}}$.

X-ray diffractometry (XRD) analyses were performed on two powdered samples (a coarser siltstone and a finer siltstone) at Pomona College in order to determine the major mineral constituents present.

RESULTS

Full tables of data from all analyses are presented in Appendix tables A1, A2 and A3. Sedimentary logs with all sample numbers are presented in Appendix figure A1.

Sedimentology

The succession at the BTB site consists of flat-lying, thinly bedded (~0.5-7 cm) mudstone, with grain size ranging from clay to coarse silt (figs. 1, 2, and 3). Medium to dark gray claystone and fine grained siltstone dominate (~79% by thickness), interbedded with thin (~1 cm) grayish-black silty claystone (~2% by thickness), medium grained siltstone (~15% by thickness), and rare coarse grained siltstone (~3% by thickness) (figs. 2 and 3).

The thin grayish-black silty-claystones tend to be the most fossiliferous beds: some are rich in pyritized or unpyritized graptolites and some yield brachiopods, orthocone nautiloids, trilobite fragments and rare bivalves (Farrell and others, 2011, fig. 2). These beds do not yield pyritized soft-tissues. They are frequently separated from overlying siltstones by a sharp or erosional contact (fig. 2; Farrell and others, 2011).

The siltstones range from massive to planar laminated or cross-laminated and occasionally show convolute or slumped laminations. Sedimentary structures at the base of the medium and coarse-grained siltstones include small-scale flute marks, and load and flame structures. Cross-lamination is generally unidirectional. Convolute lamination is confined to individual beds.

Many beds that appear massive in the field reveal very small mm-scale laminations in thin section. Normal grading is occasionally evident. Ovoid or irregularly elongate carbonate concretions (usually <10 cm maximum diameter) occur in discrete hori-

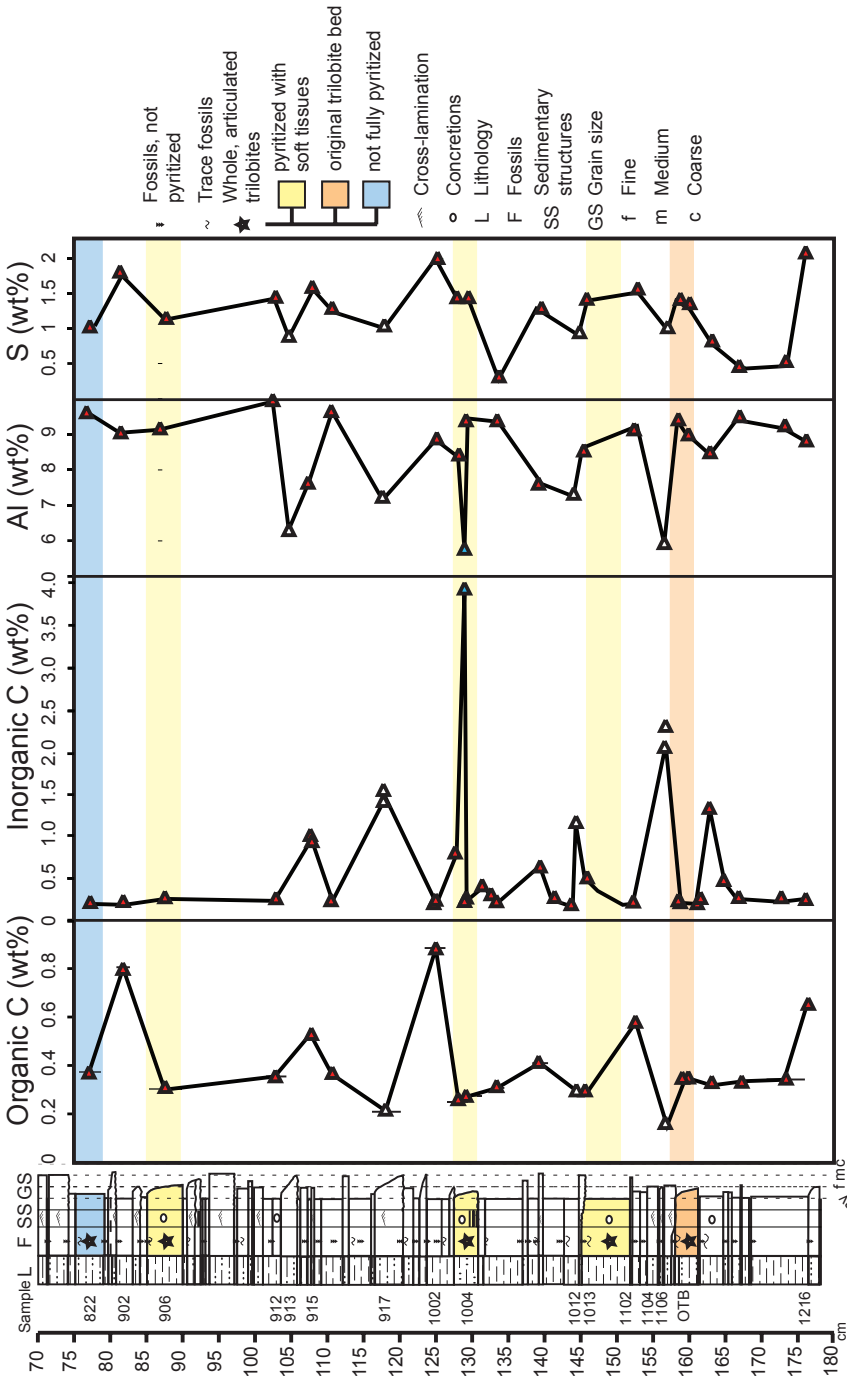

Fig. 2. Organic carbon, inorganic carbon, aluminum and sulfur content from the Walcott Quarry plotted against the stratigraphic log. Scale on the left is in centimeters below a top marker horizon. Error bars denote the stratigraphic thickness from which the samples were taken.

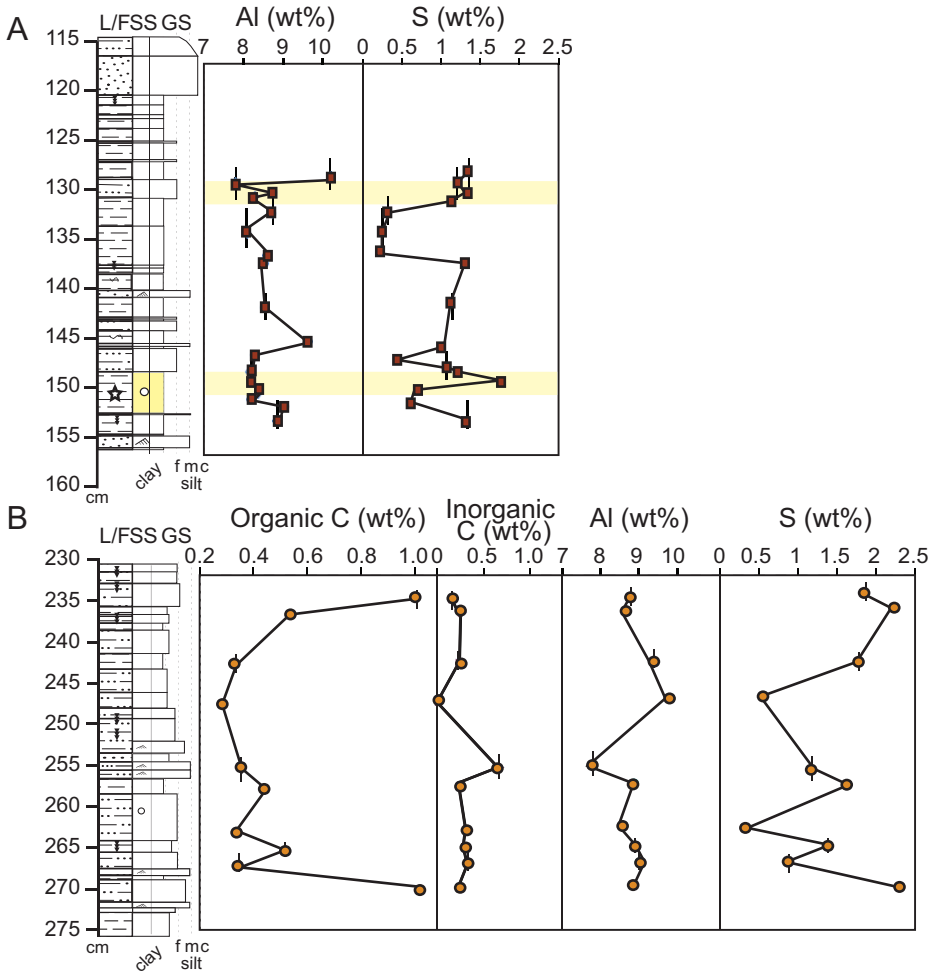

Fig. 3. (A) Aluminum and sulfur content from the Corner Quarry plotted against a stratigraphic log. (B) Organic carbon, inorganic carbon, aluminum and sulfur content from the Beecher Quarry plotted against a stratigraphic log. Scale on the left is in centimeters from a top marker horizon. Error bars denote the stratigraphic thickness from which the samples were taken. Refer to figure 2 for key to stratigraphic logs.

zons in some of the thicker mudstone beds (figs. 2 and 3). Fossils with pyritized soft-tissues are preserved within some of the thickest of these mudstone beds. Small-scale planar siltstone laminae occur near the base of these beds and most, with the exception of the OTB, yield small (on the order of 6 cm × 3 cm × 1 cm) unfossiliferous concretions. The fossils are not size-sorted and are preserved both dorsal and ventral side up (Farrell and others, 2011).

A prominent, slightly thicker (~6 cm), indistinctly laminated coarse siltstone layer is unique in the measured section and was used as a marker horizon (Farrell and others, 2009, 2011). All logs were measured from the marker horizon.

Inorganic Carbon, Aluminum, Organic Carbon, and Total Sulfur

The content of inorganic carbon (carbonate) is relatively low (generally <0.5 wt %) although outlying high values do occur, especially in concretions (4 wt % in a

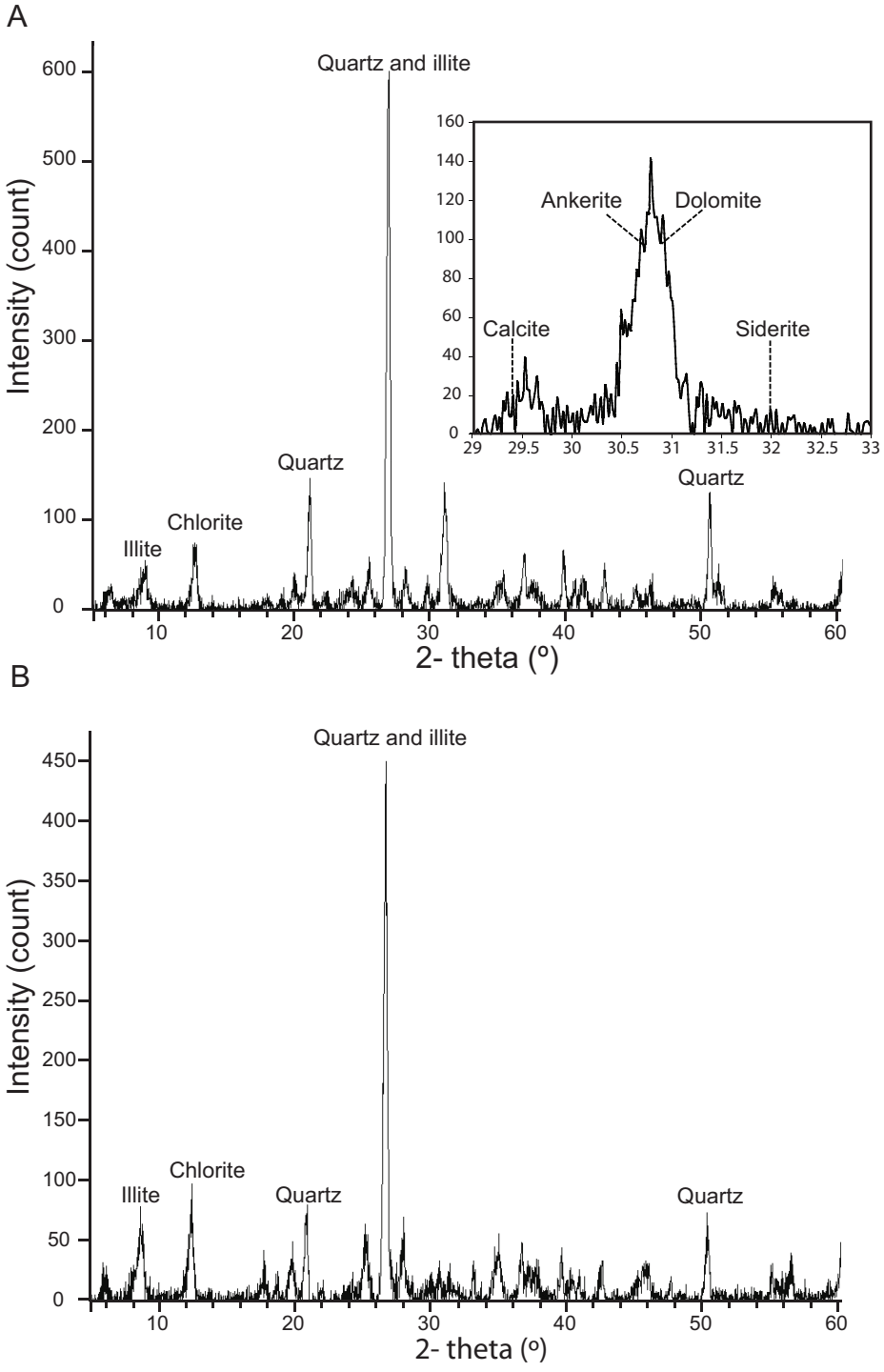

Fig. 4. XRD analyses of two beds representing a medium siltstone (A, Bed 1106) and a fine siltstone (B, Bed 1102) with the diagnostic peaks identified.

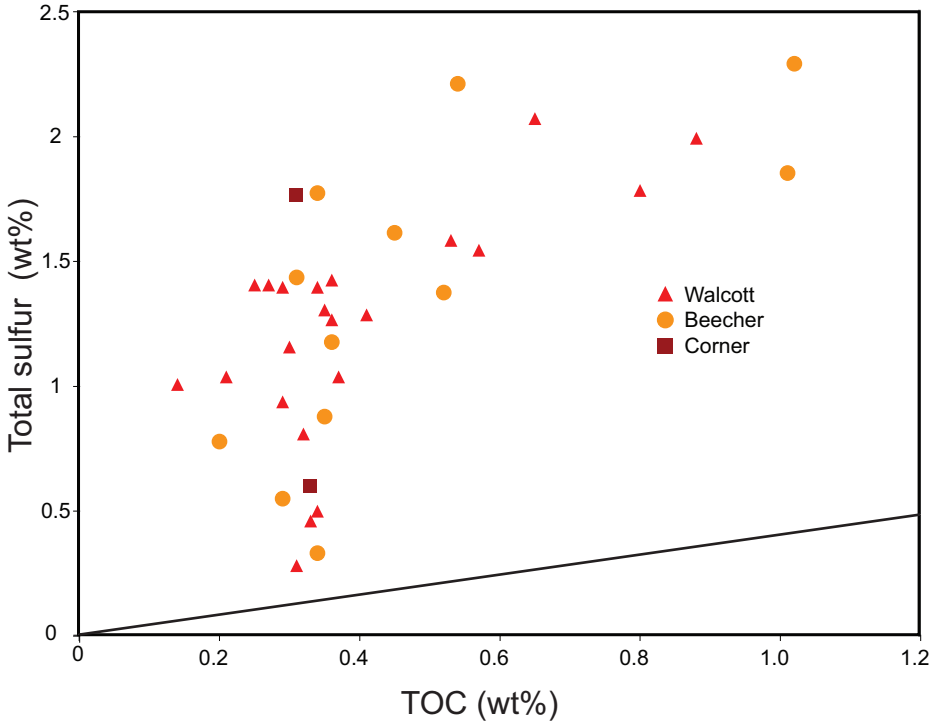

Fig. 5. Sulfur against organic carbon. The black line, with a slope of 0.4, represents the average for "normal marine" conditions in the Holocene—that is, for an oxic, saline water-column (Berner and Raiswell, 1983). Total sulfur and total organic carbon contents from this study are comparable to previously analyzed normal marine Ordovician and Silurian rocks (Raiswell and Berner, 1986).

concretion from bed 1004 and 5 wt % in a concretion from bed 912; figs. 2 and 3; Appendix table A1). Apart from concretions, the highest inorganic carbon content occurs in beds characterized by larger grain size (for example, 917, 1012, 1106; figs. 2 and 3; Appendix table A1). Where exceptionally preserved trilobites occur, but concretions are absent, inorganic carbon values are low (<0.3 wt % in the OTB; fig. 2). XRD analysis suggests that dolomite and/or ankerite are the dominant carbonate phases (fig. 4). Inorganic carbon exhibits a negative correlation with Al ($r^2 = 0.69$). Aluminum falls between 6 percent and 10 percent, consistent with average shale composite standards (WSA = 8.89%: Turekian and Wedepohl, 1961; figs. 2 and 3; Appendix table A1).

Total organic carbon (TOC) values range from 0.1–1 percent (figs. 2 and 3; Appendix table A1) but TOC may have been reduced from original levels by low-grade metamorphism (Raiswell and Berner, 1986). Beds with the highest TOC are usually dark in color and are often rich in graptolites (for example, 902, 1002, 1102; fig. 2). The TOC of beds with exceptionally preserved trilobites is 0.25 to 0.4 weight percent. Total sulfur (S_T) ranges from 0.2 to 2.3 percent (figs. 2 and 3; Appendix table A1). S_T values are frequently higher than the world shale average (WSA) of 0.24 percent (Turekian and Wedepohl, 1961). S_T and pyrite sulfur (S_{py}) are significantly correlated ($r^2 = 0.97$) (Appendix fig. A2). S_T/TOC values, which are greater than 0.4, the typical value for Holocene sediments deposited under normal marine conditions, are comparable with previously analyzed normal marine Ordovician and Silurian sedimentary rocks (fig. 5; Berner and Raiswell, 1983).

Trace Elements

Concentrations of redox-sensitive trace elements are all similar to average shale values: enrichment factors are generally around 1, and are much lower than 1 in the case of Cd (figs. 6 and 7; Appendix tables A1 and A2). Most show no correlation with Al (a proxy for detrital input in fine-grained clastic sediments) but U and V show a significant positive correlation ($p < 0.05$), and Mn an inverse correlation.

Mo/Al, Pb/Al, Ni/Al and Co/Al exhibit positive correlations with TOC, and with total S. Cd/Al, Zn/Al and Cu/Al are positively correlated in the Walcott Quarry, although not in the Beecher Quarry, and they show no significant correlation with TOC, S or inorganic carbon, although all three are most enriched where inorganic carbon content is highest (figs. 6 and 7). Mn/Al is positively correlated with inorganic carbon (Appendix fig. A3).

Mean trace element concentrations show no significant difference between the Walcott Quarry ($n = 22$) and the Beecher Quarry ($n = 12$) with the exception of U/Al, which is significantly lower in the Walcott Quarry ($t = 2.131$, $p = 0.02$, two-tailed t-test), and Mn/Al, which is significantly lower in the Beecher Quarry ($t = 2.44$, $p = 0.02$, two-tailed t-test).

The trace element concentrations in the coarsest beds in the Walcott Quarry stand out from those in other beds. Bed 1106, in particular, a 1 cm-thick cross-laminated medium-siltstone, is highly enriched in Zn (EF = 10.1) and Cu (EF = 20.6) and slightly enriched in Mn (EF = 6.0) and Cd (EF = 3.6) relative to the rest of the succession analyzed (fig. 6). Bed 1106 also yields the highest concentration of carbonate and iron, and the highest Fe_{HR}/FeT (due to a high Fe-carb content; figs. 2 and 6). Bed 1012, a thinner (~0.5 cm), cross-bedded, medium siltstone, is comparable with moderate enrichment in Cu (EF = 6.0), slight enrichment in Zn (EF = 2.0) and Mn (EF = 2.6), and high values of Fe_{HR}/FeT (fig. 6). The same signature is evident to a lesser extent in Bed 915 and Bed 917, which are also among the coarsest beds, and in the concretion from Bed 1004, which shows minor enrichments in Mn (EF = 3.5) and Cu (EF = 2.1), but little if any enrichment in Zn (EF = 1.0) (fig. 6).

Iron Speciation

Fe-ox is generally the least abundant and least variable Fe species (fig. 8), with values of 0.03–0.31 weight percent (Appendix table A1). Fe-mag is also low (0.02-0.40 wt %) and varies little (fig. 8; Appendix table A1). The concentration of Fe-ox is generally lower than that of Fe-mag in the Walcott Quarry but in the Corner Quarry and Beecher Quarry the concentrations are similar (fig. 8). Fe-carb varies from 0.19–1.95 weight percent (Appendix table A1). Fe-carb is correlated with inorganic carbon content (Appendix fig. A4), and notably higher values occur in samples from beds where grain size is slightly coarser (for example, 917, 1104b, and 1106) and in concretions (for example, in 1004; fig. 8, Appendix table A1). XRD analysis (fig. 4) showed that the composition of Fe-carb is predominantly iron-rich dolomite and/or ankerite. Siderite is not present in detectable concentrations. FeP also fluctuates considerably, from 0.02–1.83 weight percent (fig. 8; Appendix table A1). In some cases, FeP shows a clear inverse correlation with Fe-carb: such an inverse correlation occurs where Fe-carb is high in the coarser horizons but not where it is high in concretionary horizons.

Fe_{HR}/FeT values range from 0.15 to 0.58 (figs. 6 and 7; Appendix table A1). Variations in Fe-carb and FeP have the greatest influence on Fe_{HR} (fig. 8). Fe_{HR}/FeT values do not deviate significantly from a normal distribution and therefore a Student's t-test provides a valid method for evaluating differences in the mean value between sets of samples. There are no significant differences in Fe_{HR}/FeT variance among any of the quarries. Mean Fe_{HR}/FeT ($\mu(Fe_{HR}/FeT)$) is significantly higher in the Walcott

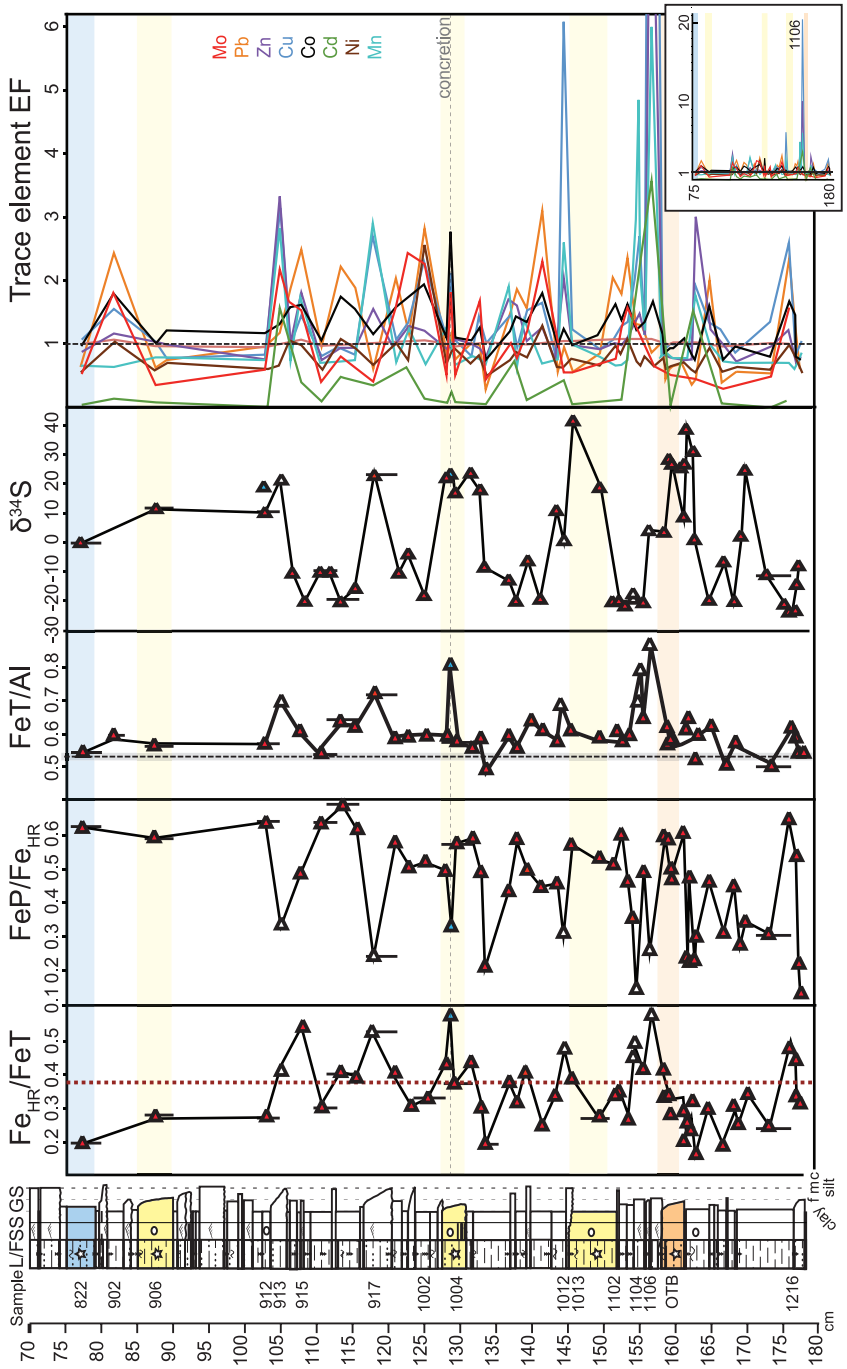

Fig. 6. Fe_{HR}/FeT, FeP/Fe_{HR}, FeT/Al, $\delta^{34}S$ and trace element enrichment factors (EF) from the Walcott Quarry. Logs (L-R): Scale from marker horizon in cm, sampling numbers (S), lithology (L)/fossils (F—see fig. 2 for full key) sedimentary structures (SS)′ and grain size (GS, c = clay, s = silt, fs = fine sand). Orange band = "original trilobite bed" (OTB), yellow band = new beds with exceptionally-preserved soft-tissues, blue band = fully articulated trilobites preserved, with no soft-tissues. Blue data points = concretions. White points = prominent siltstone layers (see text). Red dotted line = Fe_{HR}/FeT baseline (Raiswell and Canfield, 1998). Gray dotted line = average Paleozoic shale (Raiswell and others, 2008). Inset graph: trace element EF graph on a different scale to illustrate trace element EF peaks of Cu, Zn and Mn in bed 1106. Scale on left = cm from marker horizon.

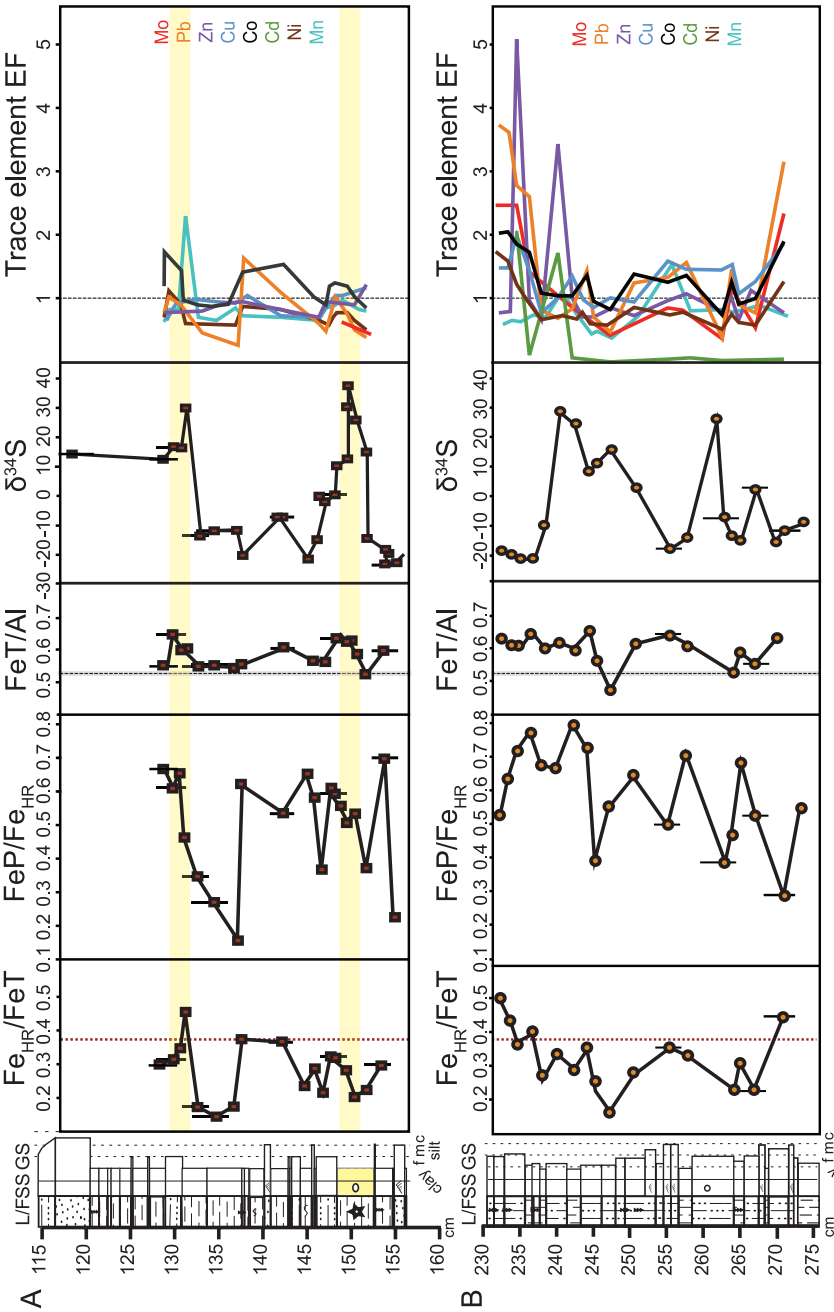

Fig. 7. (A) Fe_{HR}/FeT, FeP/Fe_{HR}, FeT/Al, $\delta^{34}S$ and trace element enrichment factors (EF) from the Corner Quarry. (B) Fe_{HR}/FeT, FeP/Fe_{HR}, FeT/Al, $\delta^{34}S$ and trace element enrichment factors (EF) from the Beecher Quarry. Logs (L-R): Scale from marker horizon in cm, sampling numbers (S), lithology (L), fossils (F—see fig. 2 for full key) sedimentary structures (SS)' and grain size (GS, c = clay, s = silt, fs = fine sand). Yellow band = new beds with exceptionally-preserved soft-tissues.

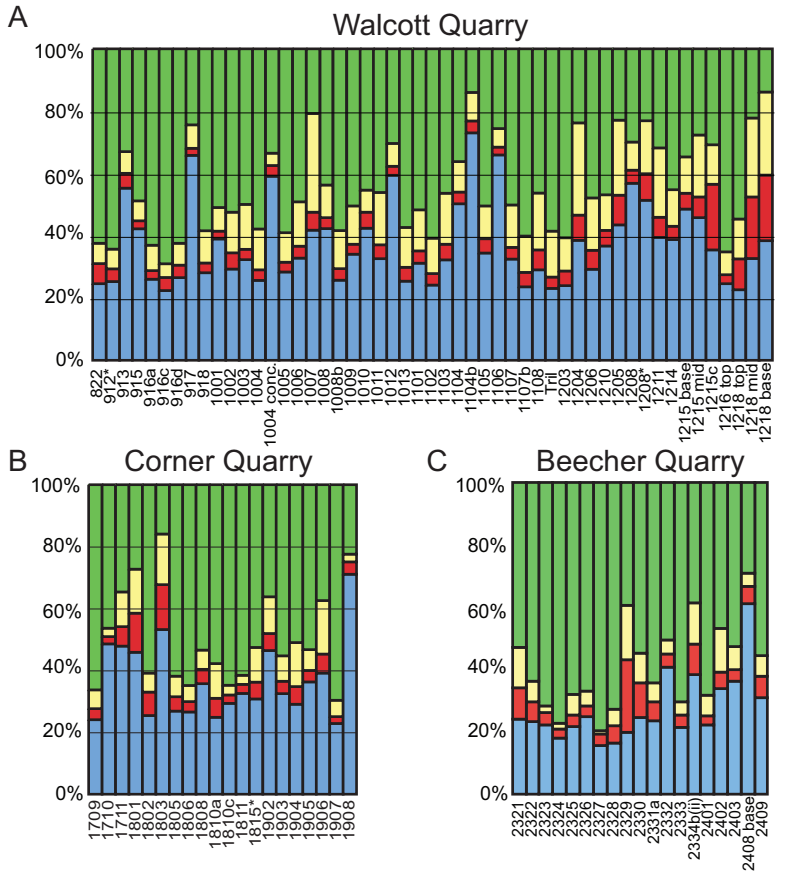

Fig. 8. Speciation of highly-reactive iron: relative amounts shown as percent of total highly-reactive iron. Blue: Fe-carb, Green: FeP, Yellow: Fe-mag, Red: Fe-ox. Sample key: * indicates samples that come from concretionary horizons but not directly from a concretion, conc. = concretion.

Quarry than in the Corner Quarry ($t = 1.20$, $p = 0.027$, two-tailed t-test). The highest Fe_{HR}/FeT values generally occur in some of the coarser horizons, and in those with highest inorganic carbon content (for example, beds 917, 1106, the concretion in 1004, figs. 2 and 6). FeP/Fe_{HR} ranges from 0.14 to 0.80 (figs. 6 and 7; Appendix table A1) and tends to be highest in some of the finer, darker beds. FeT/Al values range from 0.48 to 0.85 (figs. 6 and 7).

Iron extracted by the sodium dithionite solution alone (FeD) in a subset of samples ranged from 0.09 weight percent to 0.24 weight percent after a 2 hr extraction. The difference between the 1 hr and 2 hr extraction was small—a two-hour extraction yielded on average an additional 0.03 ± 0.01 weight percent iron (Appendix table A3).

Sulfur Isotopes

$\delta^{34}S$ of whole rock samples ranges from −24.28 permil to +42.49 permil (figs. 6, 7, and 9, Appendix table A1). There is no significant relationship between $\delta^{34}S$ and pyrite content or Fe_{HR}/FeT. $\delta^{34}S$ tends to be uniformly depleted in beds with high TOC contents, whereas a large range of values occurs in beds with lower TOC, sometimes

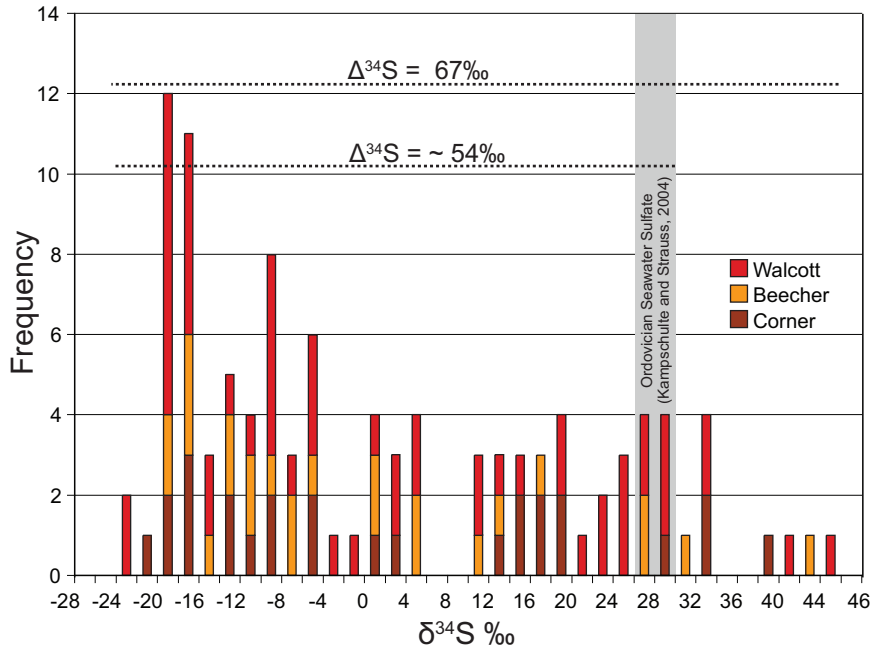

Fig. 9. Distribution of sulfur isotopic values.

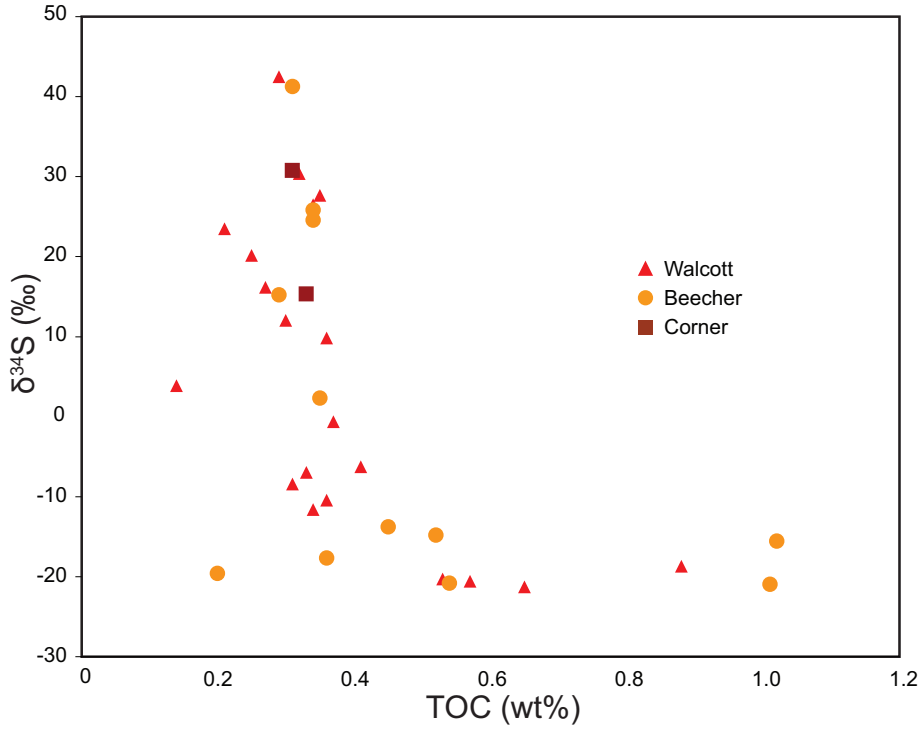

Fig. 10. Sulfur isotope values versus organic carbon content.

with a range of up to 30 permil within a single bed (figs. 6 and 10). It is noteworthy that some fraction of remobilized sedimentary pyrite was inherited from upslope (Raiswell and others, 2008). *In situ* sulfur isotopic analysis by SIMS would be necessary to determine the influence of the inherited pyrite upon bulk sediment $\delta^{34}S$ in these beds.

Trilobite Beds

Beds that yield exceptionally preserved trilobites have Fe_{HR}/FeT values ranging from 0.19 to 0.38 (figs. 6 and 7). They are generally characterized by relatively high values of FeP/Fe_{HR} showing that much of the highly-reactive iron in these beds occurs as pyrite (figs. 6 and 7). FeP is the main contributor to the relatively high Fe_{HR}/FeT in the OTB, whereas high FeP occurs alongside high Fe-carb content in some of the other beds with pyritized soft-tissues (for example, 1004; fig. 6). Beds with exceptionally preserved trilobites all have ^{34}S-enriched whole-rock values of $\delta^{34}S$ (figs. 6 and 7). The trilobite beds show no enrichment in FeT/Al or in trace elements relative to the rest of the succession (figs. 6 and 7). Although one or other of the geochemical variables may yield similar values whether or not pyritized trilobites are present, the combination of geochemical signals in the trilobite beds is rarely found elsewhere. Bed 912 is unusual in showing an almost identical chemical signature to bed 906 (fig. 6) even though excavation of it has not yielded pyritized trilobites.

DISCUSSION

Sedimentology

The majority of the siltstone and claystone beds in these quarries are interpreted as fine-grained distal turbidites, which are interbedded with thin dark-gray or black silty-claystone hemipelagic beds (see Farrell and others, 2011 for a full discussion).

Trace Elements

The redox-sensitive trace elements in these rocks are close to "average shale" composite values (Turekian and Wedepohl, 1961; Wedepohl, 1971), suggesting, in agreement with paleontological and ichnological evidence, that water-column conditions were not persistently anoxic. Rapid episodic deposition, however, may overwhelm any signal of authigenic enrichment from the water-column (Lyons and Severmann, 2006; Tribovillard and others, 2006): the correlation of U and V, in particular, with the Al content indicates that they are detrital in this succession, and are not necessarily indicative of bottom-water conditions (Dean and others, 1997; Yudina and others, 2002; Pujol and others, 2006; Tribovillard and others, 2006).

Significant enrichments of Zn, Cu and Mn, relative to average shale composite standards occur in some of the coarser-grained turbidite beds in the Walcott Quarry (915, 917, 1012, 1106; fig. 6). These turbidite beds also exhibit the highest Fe_{HR} and carbonate contents (figs. 2 and 6). Precipitation of Mn as a carbonate may occur where Mn diffuses downwards in the sediment and where pore waters are sufficiently alkaline—a situation that can occur where bottom waters are oxic and sulfate reduction occurs in the sediment (Calvert and Pedersen, 1993, 1996; Morford and others, 2001). Precipitation under such conditions is likely to result in a mixed Mn-Ca carbonate (Calvert and Pedersen, 1993). On the other hand, episodic sedimentation can cause redistribution of trace elements post-deposition—in particular, active Mn-Fe cycling can re-mobilize trace elements such as Ni, Cu, Zn, Co, and Pb (Mucci and Edenborn, 1992; Tribovillard and others, 2006). Furthermore, it is possible that the trace elements were incorporated into carbonate phases during dolomite formation and later diagenesis, perhaps due to late-stage fluid flow (Warren, 2000). The lack of volatile sulfur compounds, however, in addition to the small grain size and low permeability, suggests that late stage flow was not a significant contributing factor to trace element enrichments.

In addition to the relatively strong enrichment of Zn, Cu, and Mn, there are minor enrichments (EF between 2 and 4) of Pb, Ni, and Mo in other beds (fig. 6). These enrichments occur mostly in black or dark gray silty-claystone hemipelagic beds, or very fine grained siltstone beds that have been deposited relatively slowly (Farrell and others, 2011). Therefore, these enrichments could more accurately reflect bottom-water conditions. All three elements are correlated with organic carbon content, and enrichment could indicate that they accumulated during times of reduced bottom-water oxygen content. However, these trace element enrichments are low and possibly insignificant (for example, Turgeon and Brumsack, 2006; Ross and Bustin, 2009; Xu and others, 2012a, 2012b). In addition, enrichments of Mo up to 10 times greater than average shale have been measured in sediments deposited under a dysoxic water-column, where sulfidic pore waters occur within the sediment (Lyons and others, 2009). Therefore, anoxic water-column conditions are not necessary to account for these small enrichments relative to average shale.

The trilobite beds, which were rapidly deposited and are relatively low in organic carbon content and fine-grained, have no trace element enrichments, with the exception of the single concretion analyzed (from bed 1004). The concretion has a similar pattern of trace element enrichment to the coarser-grained turbidites that contain carbonate cements, and provides further evidence of remobilization of trace elements to sites where carbonate minerals precipitated during later stages of early diagenesis.

Sulfur Isotopes

In general the sulfur isotopic signature, with values across the full range of fractionation, is consistent with pyrite formation within the sediment porewaters, under an oxic or dysoxic water-column, where the flux of sulfate into the porewaters was predominantly controlled by variable rates and sedimentological conditions (Bloch and Krouse, 1992; Canfield and Thamdrup, 1994; Habicht and Canfield, 1997; Werne and others, 2002; Goldhaber, 2003 and references therein; Sageman and Lyons, 2003; Bickert, 2006 and references therein; Lyons and others, 2009). ^{34}S-depleted values in the succession investigated occur consistently in beds with the highest organic carbon content. In contrast, beds with lower organic carbon yield a wide range of sulfur isotopic values (fig. 10). Beds with high organic carbon are characterized by abundant poorly-oriented graptolites and a low-diversity benthic fauna on the bedding surface, which is consistent with lower sedimentation rates and accumulation in dysoxic bottom waters between episodes of event-driven sedimentation (for example, 1002, 1102, and 1216; Farrell and others, 2011). Beds with ^{34}S-enriched isotopic values, in contrast, are likely the result of sulfate reduction and sulfate restriction following rapid deposition, where sulfate-reducing bacteria were forced to use all available sulfate (Bloch and Krause, 1992; Canfield and others, 1992; Lyons, 1997; Raiswell, 1997; Gaines and others, 2012). These intervals include beds with exceptionally preserved trilobites, as well as coarser siltstone turbidites and concretions (fig. 6).

The consistently enriched sulfur isotopic values in beds with pyritized trilobites indicate that pore water sulfate became limited while sulfate reduction was taking place. However, the range of values is large within some beds (for example, from 3‰ to 31‰ within the OTB; fig. 6; Appendix table A1), suggesting a progression from relatively open-system to more closed-system conditions in some of the beds with pyritized trilobites. δ^{34}S of pyrite associated with trilobites in the OTB has an even larger range—from −3 permil to +21 permil in pyrite associated with the exoskeleton, and from +10 permil to +27 permil in pyrite associated with the limbs (Briggs and others, 1991, fig. 2) indicating that pyritization of soft tissues started early, when sulfate was more abundant, and continued as the system became closed (Briggs and others,

1991). Some of the values in the sampled interval (up to 42‰) are higher than those for average seawater, which ranged from around +30 permil in the early Ordovician to around +24 permil in the late Ordovician (Kampschulte and Strauss, 2004; fig. 9). ^{34}S-enriched values also occur in beds with concretions, even where these do not yield pyritized trilobites (912, fig. 6). These high values suggest that pyrite in concretions formed relatively late, when sulfate was depleted, with residual sulfate sourced from porewaters or even from beds below, after fractionation had removed the lighter isotopes (Briggs and others, 1991, 1996). The isotopic contribution of remobilized pyrite inherited from upslope to the bulk sedimentary δ^{34}S remains uncertain. Enriched δ^{34}S may also reflect, in part, an initial concentration of seawater sulfate lower than that of today (Gill and others, 2007, 2011; Canfield and Farquhar, 2009).

Iron Speciation

The Walcott Quarry section, which was analyzed in the greatest detail, shows multiple beds where $Fe_{HR}/FeT > 0.38$, indicating anoxic water-column conditions, in conflict with the nearly continuous presence of an in situ benthic fauna (Farrell and others, 2011). In fact, the geochemical signature appears inversely correlated with paleontological evidence: beds dominated by planktonic graptolites with only small benthic brachiopods yield lower Fe_{HR}/FeT values than samples with a better developed benthic fauna, which should indicate higher benthic oxygen concentrations. Paleontological and geochemical data integrate over slightly different time-scales, and it is possible that the two records may not perfectly match on a bed-by-bed basis while still retaining faithful chronicles of the redox history. Furthermore, rapid deposition of turbidites can dilute highly-reactive iron contents (Raiswell and Canfield, 1998; Lyons and Severmann, 2006). The present study, though, demonstrates that not only the beds yielding pyritized soft-tissues, but also the majority of the other sediments were deposited under turbiditic influence. Furthermore, the general bias associated with turbidites is one of dilution (Raiswell and Canfield, 1998; Lyons and Severmann, 2006), rather than the enrichment present in the Walcott Quarry.

In the Walcott Quarry, the strongest enrichments in Fe_{HR}, and in the trace elements Zn, Cu and Mn, occur in beds with the highest carbonate contents, including the coarser turbidite beds and the concretion sampled (fig. 6). These enrichments may be due in part to the fact that the siltier and more carbonate-rich beds may have less lithogenous iron, and therefore less FeT than the more clay-rich mudstones. Furthermore, it is clear that later stage processes during early diagenesis can account for Fe_{HR} enrichment in these samples, by relocation of Fe(II) in solution from host sediments to sites where diagenetic processes were sustained, in concretions or siltstone beds with authigenic cements. Enrichment may have resulted from simple diffusion, from injection of pore waters into more porous silt beds and concretion frameworks during mudstone compaction, or some combination of the two processes. The same mechanism can also explain the relocation of trace elements into these horizons in anoxic pore waters of the burial environment. Enriched sulfur isotope values provide evidence of later stage diagenetic activity in the Fe_{HR}/FeT enriched intervals. Further analysis of carbon and oxygen isotopes of the carbonate cements could help determine the timing of carbonate formation in these sediments. Nevertheless, concretions and the beds that contain them, which were likely influenced by variable sedimentation rates (for example, Brett and others, 2008), are clearly not suitable for interpreting bottom-water redox conditions, as reactive iron components can be redistributed during concretion formation (Raiswell, 1988). Our results suggest that cemented intervals in coarser grained sediments within mudstone successions should be regarded with similar caution.

FeT/Al is a less sensitive indicator of anoxia than Fe_{HR}/FeT (Anderson and Raiswell, 2004; Lyons and Severman, 2006), however, it is less likely to be affected by

the effects of diagenesis and metamorphism (Raiswell and others, 2008). The FeT/Al values in these sections are on average slightly, but not significantly, higher than average Paleozoic shale values (figs. 6 and 7; Raiswell and others, 2008). Al is considered representative of the alumino-silicate fraction in fine-grained sediments and therefore it accounts to some extent for the variable sedimentation rate and dilution by biogenous sediment (Anderson and Raiswell, 2004; Lyons and Severman, 2006 and references therein). The FeT/Al signature matches the Fe_{HR}/FeT signature, when the highest values are in beds enriched in Fe-carb, but not when there are relatively high amounts of FeP. Therefore, enrichment in Fe/Al may be due to a combination of higher iron-carbonate content and simultaneously lower Al content in these carbonate-cemented siltstones and in the concretions.

Environmental Interpretation

The combined geochemical and paleontological signal from these quarries can be compared to that obtained in a similar study of Devonian strata in upstate New York (Boyer and others, 2011). Those strata contain a low-diversity assemblage of small trace fossils (primarily *Planolites*) and a low-diversity, high dominance body fossil assemblage—a classic dysaerobic signal (Savrda and Bottjer, 1991). Geochemical data from the same sections showed Fe_{HR}/FeT values less than 0.38, low to no enrichments in FeT/Al, Mo and Mn, and pyrite sulfur isotope values in the range of -10 to $-20^{0/00}$. This prompted Boyer and others (2011) to consider those Devonian sediments to be deposited under a dysoxic water-column, with rare to absent short-lived anoxic episodes. Furthermore, although they noted that available geochemical proxies are well-suited to distinguishing between oxic and anoxic conditions, and between a ferruginous or euxinic anoxic water-column, they had trouble using such proxies to distinguish changes in relative oxygen levels within a dysoxic water-column even though they were clearly recorded by paleontological evidence. The Ordovician strata investigated here likely represent a similar case with oxygen levels that fluctuated, sometimes to low levels, but without the development of truly anoxic conditions. Unlike the Devonian sediments, which were deposited relatively slowly and without the influence of event-driven sedimentation (Boyer and others, 2011), however, the geochemical signal in these sections is complicated by relatively high and variable sedimentation rates.

Despite an overall dysoxic signal from both paleoecological and geochemical data, certain inconsistencies remain. First, the Walcott Quarry and the Corner Quarry overlap in their stratigraphy, with both covering the interval 115 to 160 cm below the marker bed, but they show slightly different iron speciation signatures. The Fe_{HR}/FeT values of the Corner Quarry samples are essentially all less than or equal to 0.38 (fig. 7), whereas some of the Walcott Quarry samples exceed this threshold (fig. 6). Secondly, the average Fe_{HR}/FeT values for the BTB site from the earlier study by Raiswell and others (2008) are considerably lower and less variable than the values found here [0.21 ± 0.03 in Raiswell and others (2008), 0.37 ± 0.11 in this study], irrespective of which quarry is considered, although the average FeT/Al is similar in both studies [0.61 ± 0.04 in Raiswell and others (2008), 0.60 ± 0.06 in this study]. Raiswell and others (2008) used a set of samples collected from the Walcott Quarry.

Differences between the Corner and Walcott Quarry could be the result of weathering. As sections are exposed along a riverbank, all samples are weathered to some degree, although care was taken to analyze only clean gray samples. The Corner Quarry and Beecher Quarry seem to have experienced more weathering than the Walcott Quarry, as they were in closer proximity to the soil surface before excavation (fig. 1). The primary effect of weathering, however, is to change Fe^{2+} phases to iron oxides (Canfield and others, 2008), which changes the partitioning of iron within the Fe_{HR} pool but does not enrich it. A second possibility is secondary fluid flow resulting

in additional iron carbonate enrichments in the Walcott Quarry. However, as the quarries are only ~10 meters apart and the beds are flat-lying and can be traced along the outcrop, it is unlikely that secondary fluid flow would affect one and not the other. The exact reason why the Walcott Quarry is more enriched than the other two quarries remains unclear but it may simply be a matter of sampling. When only values from that part of the Walcott Quarry succession that overlaps with the Corner Quarry are compared, and bed 1012 and concretions, which were not sampled in the Corner Quarry, are omitted, there is no significant difference between the two quarries ($p = 0.06$). Furthermore, the pattern of enrichment is more or less the same, with high values of Fe_{HR}/FeT in the thick siltstones with concretions, and in the coarser-grained beds. This is the first study to systematically investigate iron speciation along strike, and further detailed studies in other localities may help explain how and when heterogeneous signals can occur.

Regarding the differences between the iron speciation data obtained in this study and those reported by Raiswell and others (2008), it should be noted that although the averages are different, individual points analyzed in this study overlap with the values in the previous study. The differences in averages may simply reflect differences in sampling. However, the section from Raiswell and others (2008) overlaps exactly with a subset of the section sampled in this study (~6 cm below to ~6 cm above the OTB; Raiswell and others, 2008). Furthermore, both studies have the same average value of FeT/Al. This suggests that the difference may be attributed to reactive iron extraction methodology. While the present study follows Poulton and Canfield (2005) in defining Fe_{HR} as the sum of FeP + Fe-carb + Fe-ox + Fe-mag (the last three extracted sequentially), the study of Raiswell and others (2008) used the methodology of Canfield (1989) and Raiswell and others (1994) where Fe_{HR} is defined as FeP plus FeD (that is, iron extracted with the same dithionite extraction as Fe-ox, but without using an acetate extraction first or oxalate after). Furthermore, there is some ambiguity regarding the dithionite extraction time used to determine FeD. Following Poulton and Canfield (2005), the dithionite extraction in this study ran for 2 hours. However, Raiswell and others (2008) cited both Canfield (1989) and Raiswell and others (1994) in their methodology, but the dithionite extraction ran for 1 hour in the former and 2 hours in the latter.

To date, no study has directly compared samples analyzed under these two extraction methodologies. In order to explore the difference between these two extraction methods, we analyzed a subset of samples using the original methodology of Raiswell and Canfield (1998) and compared the results with those obtained with the sequential extraction methodology of Poulton and Canfield (2005). One-hour and two-hour sodium dithionite extractions yielded essentially the same values (Appendix table A3). These values were higher by varying amounts (28 to 75% change) than those for dithionite-extractable iron in the sequential extraction (fig. 11A; Appendix table A3). Higher values for FeD compared to Fe-ox are not surprising, as it has been shown that the sodium dithionite solution extracts some carbonate iron (up to ~22% siderite and ~14% ankerite in pure mineral extractions; Raiswell and others, 1994). When combined with FeP, however, the Fe_{HR} values obtained using the original iron extraction methodology of Raiswell and Canfield (1998) are systematically lower than those using the sequential methodology of Poulton and Canfield (2005) (fig. 11B). This is also consistent with our understanding of sodium-dithionite extraction efficiencies on iron carbonate and magnetite: while the dithionite solution has been shown to extract some carbonate iron (Raiswell and others, 1994) and up to 5 percent of magnetite iron (Poulton and Canfield, 2005) in pure-mineral extractions, it leaves the majority of those phases unaffected (hence its value as a method for determining iron oxide concentrations; for example, Poulton and Canfield, 2005). Thus, the difference

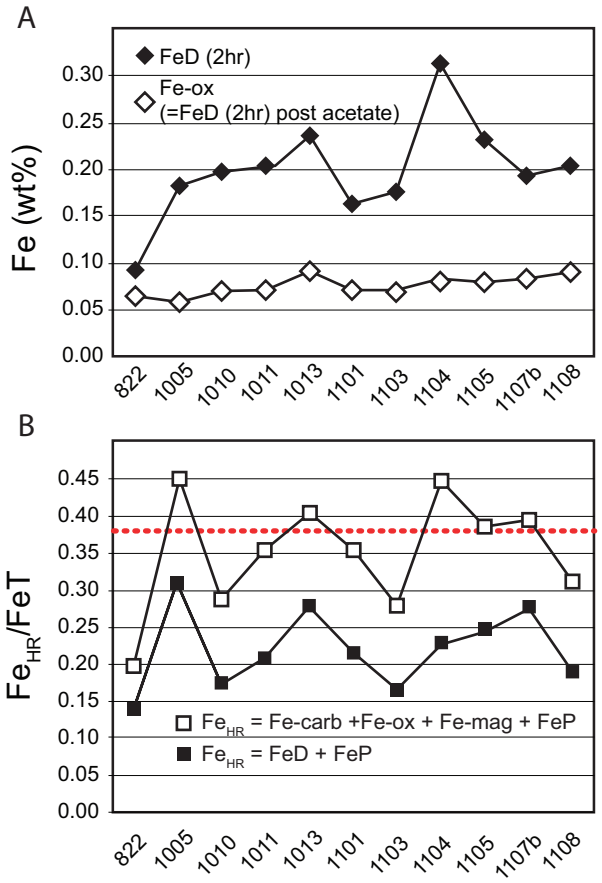

Fig. 11. (A) Dithionite-extractable iron (FeD) and dithionite-extractable iron extracted after an acetate extraction (Fe-ox). (B) Fe_{HR}/FeT in a subset of samples from the Walcott Quarry determined i) using the method of Raiswell and Canfield (1998), where Fe_{HR} is operationally defined as FeD + FeP, and ii) using the sequential extraction method of Poulton and Canfield (2005), where Fe_{HR} is operationally defined as Fe-carb + Fe-ox + Fe-mag + FeP.

between the average Fe_{HR}/FeT values obtained by Raiswell and others (2008) and those in this study almost certainly reflects differences in extraction methodology as opposed to sampling effects.

The different Fe_{HR}/FeT results obtained using these two extraction methodologies have implications for comparing iron speciation values generated by sequential extraction with the modern (Raiswell and Canfield, 1998), Phanerozoic (Poulton and Raiswell, 2002) and Paleozoic (Raiswell and others, 2008) oxic/anoxic baselines, as those baselines were obtained using the original extraction technique of Raiswell and Canfield (1998). The assumption implicit in comparing values obtained from a sequential extraction with those that make up these baselines must be that the same Fe_{HR} number would be obtained if these baseline sample sets were re-analyzed using the sequential technique. In the case of the modern baseline (that is, $Fe_{HR}/FeT > 0.38$ indicates anoxic bottom water) this assumption is likely to hold true. Modern sediments do not contain high amounts of carbonate iron, due to higher sulfate concentrations in the modern ocean, which lead to efficient sulfidization of these highly-reactive

phases. Furthermore, in general magnetite is a very minor component of most sediments (for example, 0.05 to 0.01 wt % in the FOAM sediments from Long Island Sound; Canfield and Berner, 1987). The modern oxic baseline does need to be re-investigated, especially in depositional settings that host high quantities of siderite (such as the Amazon mobile mud belt; Aller and others, 2010), or magnetite (such as sediments sourced from volcanic arc systems), but in general the result is likely to qualify rather than fundamentally change the value. In the meantime sequential iron extraction values can still be compared with the modern baselines.

Phanerozoic oxic baseline datasets, however, may show a different pattern upon re-analysis with the sequential technique. Samples that preserve paleontological evidence of a dysoxic signal and therefore should be characterized as "oxic," may contain appreciable amounts of iron carbonate and magnetite (Coleman, 1985; Bloch and Crouse, 1992; Curtis, 1995; Maquaker and others, 1997). Lower sulfate concentrations in Paleozoic oceans (Gill and others, 2007, 2011; Canfield and Farquhar, 2009) could have resulted in low sulfide concentrations during diagenesis and, hence, relatively common iron-carbonates and magnetite. In this scenario it is likely that an oxic baseline for ancient sediments would shift upwards when these phases are taken into account. Consequently, comparison of values of Fe_{HR}/FeT obtained with the sequential extraction methodology in ancient sediments with Phanerozoic baseline datasets (for example, Poulton and Raiswell, 2002; Raiswell and others, 2008) obtained with the original extraction methodology is complex. The baseline threshold values require re-evaluation using the sequential method. Furthermore, it seems likely that the difference between modern and Paleozoic oxic averages (for example, Raiswell and others, 2008) may be due partly to under-estimation of the highly-reactive pool in the ancient rocks, in addition to conversion of reactive forms to unreactive forms such as chlorite during burial diagenesis and metamorphism (Poulton and Raiswell, 2002).

In sum, the overall signal based on this multi-proxy approach points towards a geochemical signature dominated by episodic sedimentation, deposited under a predominantly dysoxic water-column, with potentially brief and rare development of ferruginous anoxic conditions. The discrepancy between data from the Corner and Beecher Quarries and the Walcott Quarry may be explained by sampling and the effects of differential diagenesis. The difference in iron speciation averages between this study and Raiswell and others (2008) are likely due to differences in extraction methodology.

Geochemical Signatures of Soft-tissue Preservation

Conditions suitable for soft tissue pyritization were established in relatively thick (~4-7 cm) turbidite-deposited fine-siltstone to claystone beds, often in association with small carbonate-rich concretions (Farrell and others, 2009, 2011). The trilobite beds that yield pyritized soft tissues also contain pyritized burrows, which are mostly parallel to bedding and more abundant at the tops of beds. The size (<1 cm), depth and low-diversity of the trace fossils and their replacement in pyrite indicate that post-depositional conditions in the water-column were dysoxic (Farrell and others, 2009, 2011). Pyritized soft-tissues are not present in medium or coarse siltstones, in hemipelagic or hemiturbiditic beds, or in thinner mudstone beds.

These trilobite beds show intermediate to high concentrations of pyrite and variable amounts of Fe-carb. The pyrite content indicates that sulfate reduction was active, albeit in microenvironments, and pyrite may have continued to form in the sediments after soft-tissues were preserved (Briggs and others, 1991). Some pyrite was inherited from upslope, having formed prior to turbidite re-suspension and re-deposition (Raiswell and others, 2008). The iron-enriched carbonate concretions, which occasionally have a pyritic core, and the Fe-carb values in non-concretionary sediment indicate that sulfidic conditions did not become established in the porewa-

ters. Ankerite has been reported from around a pyritized trilobite in the OTB (Buck, ms, 2004), providing further evidence for iron-dominated porewaters. The consistently enriched sulfur isotopic values in beds with pyritized trilobites indicate that pore water sulfate became limited while sulfate reduction was still ongoing. The $\delta^{34}S$ of pyrite associated with trilobites (Briggs and others, 1991) indicates that soft-tissue replacement started in the earlier stages of sulfate reduction while sulfate concentrations were still higher and continued as conditions became closed. Although similarly enriched $\delta^{34}S$ of sedimentary pyrite has also been noted in beds with Burgess Shale-type preservation (Gaines and others, 2012) sulfate restriction was shown to have occurred very quickly following deposition, resulting in a different taphonomic mode of Burgess Shale-type fossils. While the preservation of these carbonaceous fossils required very early retardation of microbial activity in the sediments, preservation of soft tissues in pyrite requires that porewaters in the early burial environment maintained enough sulfate to promote rapid mineralization resulting from the metabolic activity of sulfate reducers.

Bed 822 from the Walcott Quarry yields fully articulated trilobites but no soft tissues are preserved—clearly some of the key components necessary for early pyritization were missing. The content of highly-reactive iron is slightly lower than in the OTB and bed 1004 and the pyrite is more ^{34}S-depleted. However, the geochemical signature in bed 906, which does preserve soft tissues, is almost identical to that of 822. Bed 822 is slightly thinner than the other trilobite beds, although grain size is similar. This suggests that a combination of a lower concentration of reactive iron and relatively open conditions, which would have promoted the escape of sulfide as well as the diffusion of sulfate into the sediments, prevented the early precipitation of iron sulfides around soft-tissues.

CONCLUSION

Fully articulated trilobites are preserved in thicker event-deposited mudstones. Diagenesis in the source area and subsequent physical reworking of the sediment reduced the amount of metabolizable organic carbon in turbidite-deposited beds, and resulted in iron-rich conditions in pore waters, partly due to the oxidation of pyrite during transport. This created the two primary conditions necessary to confine pyrite formation to the organic matter of the fossil carcasses (Briggs and others, 1991; Raiswell and others, 2008). The episodic depositional regime caused remobilization of iron fractions and localized precipitation of pyrite (for example, Brett and others, 2008), although the distribution of carbonate-associated iron and trace element concentrations may have been affected by later diagenesis. Periods of slower deposition allowed burrowing organisms to become established and to concentrate more labile organic matter (in burrow linings), which provided an additional locus for pyritization. Pyritization of soft tissues did not occur in coarser siltstone beds, in mudstone intervals where sedimentation rates were slow, or where the thickness of event-deposited sediment was insufficient to inhibit diffusion early enough in the diagenetic succession. The multi-proxy geochemical data are generally consistent with paleoecological inferences (Farrell and others, 2011) in suggesting predominantly oxygenated conditions, although brief periods of anoxic, ferruginous conditions may have occurred. Conclusive evidence of persistent non-sulfidic anoxia in the water-column is absent. Bottom water conditions were clearly not euxinic during deposition of the trilobite beds because sulfidic pore-waters would have prevented localized pyritization. Fully oxic conditions, on the other hand, would have facilitated deep and extensive bioturbation, which would have disturbed the carcasses and promoted degradation, likewise preventing the preservation of soft-tissues.

ACKNOWLEDGEMENTS

We thank D. Canfield for many helpful discussions and comments, M. Martin, T. Whiteley, J., and S. Koziarz, the Stark family and others for help with fieldwork, A. Fulton, K. Metcalfe, C. Sendek, G. Olack, and L. Saling for help with chemical analyses, D. Johnston for lab assistance and discussion, and S. Poulton, R. Raiswell and one anonymous reviewer for helpful comments. This project was supported by student research grants from the Yale Institute of Biospheric Studies, Geological Society of America, Paleontological Society and the International School of Aquatic Sciences, Denmark.

Appendix

Full tables of data from all analyses are presented in Appendix tables A1, A2, and A3. Sedimentary logs with all sample numbers are presented in Appendix figure A1. Plots of pyrite sulfur weight percent versus total sulfur weight percent, inorganic carbon versus Mn/Al and inorganic carbon versus Fe-Carb are presented in figures A2, A3, and A4 respectively.

Table A1

Chemical data for samples from the Walcott Quarry (WQ), Corner Quarry (CQ) and Beecher Quarry (BQ), Enrichment Factors relative to "World Shale Average" (Turekian and Wedepohl, 1961; Wedepohl, 1971). EF(trace element) = (X/Al)sample/(X/Al)average shale

Sample	Fe-carb	Fe-ox	Fe-mag	FeP	FeT	Inorg-C	TOC	S	Al	$\frac{Fe_{HR}}{FeT}$	$\frac{FeP}{Fe_{HR}}$	$\frac{FeT}{Al}$	$\delta^{34}S$	Mo	U	V	Zn	Pb	Cu	Cd	Ni	Co	Mn
	wt%												permil	Enrichment factor									
WQ																							
822	0.25	0.07	0.07	0.63	5.19	0.19	0.37	1.04	9.62	0.20	0.62	0.54	-0.61	0.49	1.00	1.14	0.88	0.64	1.06	0.06	0.54	0.92	0.64
902					5.39	0.20	0.80	1.79	9.01			0.60		1.79	1.07	1.18	1.16	2.43	1.55	0.16	1.03	1.76	0.62
906				1.01	5.39	0.27	0.30	1.16	9.15			0.59	12.05	0.33	0.97	1.13	1.05	0.62	1.03	0.11	0.59	0.97	0.77
YPM[1]	0.28	0.06	0.21	0.80	4.97			0.90	8.41	0.27	0.59	0.59	10.78	<0.8		1.21	0.99	0.74	0.78		0.70	1.17	0.78
912*				0.56		0.50							18.41										
912	0.38	0.06	0.10	0.96	5.71	0.23	0.36	1.43	9.94	0.26	0.64	0.57	9.85	0.59	0.94	1.15	0.75	0.95	0.83	0.04	0.59	1.13	0.74
913	0.98	0.08	0.12	0.59	4.36			0.70	6.27	0.41	0.33	0.70	20.99	2.18		1.04	3.33	1.13	3.12	1.60	0.67	1.27	2.82
914	0.81		0.24	1.01	4.98			1.30	8.29			0.60	-10.70	1.65		1.21	1.02	1.88	0.98		1.04	1.64	0.71
915	1.03	0.06	0.16	1.19	4.59	1.00	0.53	1.59	7.64	0.53	0.49	0.60	-20.27	1.53	1.10	1.15	1.81	2.49	1.44	0.42	0.98	1.62	1.74
916a	0.40	0.04	0.13	0.98	5.19	0.22	0.36	1.27	9.65	0.30	0.63	0.54	-10.43	0.39	0.97	1.14	0.75	0.95	0.80	0.07	0.59	1.06	0.69
916b				1.02									-11.02										
916c	0.50	0.09	0.10	1.55	5.61			1.80	8.83	0.40	0.69	0.64	-20.45	0.77		1.20	0.93	2.21	0.92	0.50	1.07	1.75	0.68
916d	0.57	0.09	0.15	1.35	5.47			1.60	8.75	0.39	0.62	0.63	-16.22	<0.8		1.17	0.94	1.88	0.84		0.91	1.55	0.73
917	1.83	0.06	0.21	0.68	5.20	1.54	0.21	1.04	7.15	0.53	0.24	0.73	23.48	0.40	1.01	1.03	1.58	0.60	2.71	0.34	0.66	1.15	2.90
918	0.57	0.06	0.21	1.19	5.03			1.30	8.72	0.41	0.58	0.58	-10.57	1.57		1.18	0.91	2.04	1.06		1.02	1.56	0.70
1001	0.58	0.04	0.11	0.75	4.93			1.00	8.41	0.30	0.51	0.59	-4.32	2.44		1.04	1.28	1.16	1.34	0.66	0.73	1.22	1.24
1002	0.50	0.09	0.22	0.90	5.25	0.20	0.88	2.00	8.85	0.33	0.52	0.59	-18.71	2.26	1.06	1.18	1.21	2.86	2.28	0.16	2.61	1.94	0.68
1003	0.67	0.07	0.30	1.04	4.97	0.80	0.25	1.41	8.43	0.42	0.50	0.59	20.14	0.49	1.00	1.12	0.91	0.80	1.05	0.09	0.68	1.09	1.24
1004	0.50	0.07	0.26	1.13	5.28	0.23	0.27	1.41	9.34	0.37	0.58	0.57	16.19	0.50	0.98	1.11	1.07	0.76	1.07	0.11	0.93	1.10	0.67
1004*	1.53	0.09	0.10	0.87	4.52	3.91			5.66	0.57	0.33	0.80	23.20	1.81	0.89	1.40	1.02	1.14	2.11		0.96	2.77	3.48
1005	0.54	0.06	0.18	1.12	4.45	0.41		1.30	7.93	0.42	0.59	0.56	23.12	<0.9		1.35	1.00	1.01	0.82		0.69	1.06	0.80
1006	0.46	0.05	0.20	0.68	4.71	0.31		1.40	8.15	0.30	0.49	0.58	17.58	1.68		1.26	0.93	0.98	1.43		0.80	1.26	0.75
1007	0.36	0.05	0.27	0.18	4.56	0.19	0.31	0.28	9.36	0.19	0.21	0.49	-8.44	0.43	1.03	1.16	0.78	0.28	0.99	0.07	0.50	0.70	0.67
1008	0.62	0.05	0.15	0.64	3.95			0.70	6.74	0.37	0.44	0.59	-13.18	1.01		1.10	1.71	1.52	1.47	0.66	0.74	1.18	1.91
1008b	0.39	0.06	0.19	0.88	4.91			1.50	8.81	0.31	0.58	0.56	-19.69	0.78		1.22	1.60	1.87	0.94	0.76	0.88	1.43	0.64
1009	0.66	0.06	0.24	0.97	4.78	0.64	0.41	1.29	7.50	0.40	0.50	0.64	-6.26	1.19	0.99	1.06	1.05	1.56	1.53	0.13	0.78	1.32	1.38
1010	0.58	0.07	0.10	0.62	5.41	0.27		1.70	8.89	0.25	0.45	0.61	-19.68	2.31		1.10	1.26	3.10	1.64		1.29	1.79	0.69
1011	0.53	0.07	0.27	0.75	4.91	0.18		0.70	8.67	0.33	0.46	0.57	10.72	<0.8		1.19	0.79	0.56	0.77		0.63	0.97	0.74
1012	1.41	0.07	0.18	0.72	5.05	1.19	0.29	0.94	7.35	0.47	0.30	0.69	-3.84	0.56	1.05	1.06	2.04	0.95	6.05	0.45	0.62	1.24	2.59
1013	0.52	0.09	0.26	1.17	5.16	0.51	0.29	1.40	8.51	0.39	0.57	0.61	42.49	0.54	1.04	1.18	0.98	0.53	1.23	0.08	0.76	0.98	0.99
YPM[2]	0.32	0.07	0.24	0.72	4.99			0.90	8.40	0.27	0.53	0.59	19.02	0.81		1.22	0.91	0.85	0.94		0.65	1.11	0.78
1101	0.56	0.07	0.24	0.92	5.48	0.18		1.60	8.92	0.33	0.52	0.61	-20.55	0.77		1.17	1.02	2.04	1.06		0.97	1.63	0.66
1102	0.43	0.07	0.20	1.08	5.20	0.20	0.57	1.55	9.13	0.34	0.61	0.57	-20.55	1.25	1.05	1.14	0.98	1.79	1.27	0.12	0.84	1.38	0.65

Table A1

(continued)

Sample	Fe-carb	Fe-ox	Fe-mag	FeP	FeT	Inorg-C	TOC	S	Al	$\frac{Fe_{HR}}{FeT}$	$\frac{FeP}{Fe_{HR}}$	$\frac{FeT}{Al}$	$\delta^{34}S$	Mo	U	V	Zn	Pb	Cu	Cd	Ni	Co	Mn
	wt%												permil	Enrichment factor									
WQ																							
1103	0.44	0.07	0.22	0.63	5.23			1.50	8.68	0.26	0.46	0.60	-21.92	1.58		1.09	1.10	2.36	1.34		1.08	1.62	0.73
1104	1.07	0.08	0.21	0.77	4.63			0.80	6.72	0.46	0.36	0.69	-19.87	<1.0		1.03	1.36	1.32	2.03		0.72	1.25	2.97
1104b	1.63	0.09	0.20	0.31	4.58			0.60	5.79	0.49	0.14	0.79	-17.76	<1.2		1.02	1.47	1.31	2.70		0.65	1.21	4.86
1105	0.59	0.08	0.18	0.86	4.19			0.90	6.57	0.41	0.50	0.64	-20.39	<1.0		1.08	1.17	1.29	1.14		0.80	1.35	1.23
1106	1.95	0.08	0.18	0.76	5.13	2.29	0.14	1.01	5.96	0.58	0.26	0.86	3.89	0.65	1.09	0.96	10.06	0.86	20.58	3.60	0.65	1.65	6.02
1107	0.67	0.08	0.28	1.04	5.48	0.22	0.34	1.40	9.39	0.38	0.50	0.58	26.49	0.48	1.02	1.17	0.78	0.65	0.98	0.05	0.63	0.96	0.75
1107b	0.43	0.09	0.21	1.10	5.49			1.20	8.90	0.33	0.60	0.62	3.01	<0.8		1.22	0.83	1.05	1.00		0.76	1.16	0.79
1108	0.40	0.09	0.25	0.64	5.07			0.60	9.04	0.27	0.46	0.56	31.25	<0.8		1.22	0.79	0.44	0.94		0.58	0.83	0.82
Tril	0.39	0.06	0.25	0.98	5.20	0.21	0.35	1.31	8.95	0.32	0.59	0.58	27.67	0.52	0.99	1.21	0.78	0.61	0.98	0.05	0.64	0.91	0.75
1203	0.39	0.08	0.17	0.98	5.74	0.20		1.30	9.02	0.28	0.61	0.64	25.39	<0.8		1.25	0.76	0.69	1.03		0.70	1.09	0.76
1204	0.36	0.08	0.28	0.22	4.71			0.30	8.89	0.20	0.24	0.53	26.28	<0.8		1.22	0.75	0.30	0.93		0.56	0.68	0.73
1206	0.37	0.08	0.21	0.60	5.08	0.24		0.70	8.89	0.25	0.48	0.57	38.57	<0.8		1.20	0.75	0.35	0.93		0.59	0.84	0.77
1210	0.55	0.08	0.17	0.70	4.93	0.47		1.30	7.93	0.30	0.47	0.62	-19.98	<0.9		1.24	1.22	2.02	1.32		0.94	1.59	1.00
1205	0.45	0.10	0.25	0.24	4.57			0.20	8.99	0.23	0.23	0.51	0.91	<0.8		1.21	0.70	0.25	0.79		0.51	0.68	0.67
1208	0.94	0.07	0.15	0.50	5.11	1.38	0.32	0.81	8.52	0.32	0.30	0.60	30.40										
1208 (aboveconc.)	0.36	0.06	0.12	0.16	4.56			0.20	8.89	0.16	0.23	0.51	8.12	0.43	1.03	1.14	3.01	0.44	1.95	1.55	0.54	0.76	1.76
1211	0.39	0.06	0.22	0.31	4.85	0.25	0.33	0.46	9.50	0.20	0.32	0.51	-6.95	0.28	0.96	1.15	0.99	0.36	1.20	0.08	0.53	0.71	0.72
1214	0.58	0.06	0.18	0.68	4.97			0.70	8.67	0.30	0.45	0.57	-20.36	<0.8		1.21	0.72	0.56	0.87		0.62	0.97	0.70
1215 base	0.83	0.09	0.20	0.59	5.21			0.70	8.65	0.33	0.35	0.60	24.18										
1215 middle	0.57	0.08	0.25	0.34	4.90			0.40	8.51	0.25	0.28	0.58	1.29										
1215c	0.40	0.24	0.14	0.35	4.74	0.24	0.34	0.50	9.25	0.24	0.31	0.51	-11.61	0.48	0.99	1.16	0.97	0.52	1.36	0.02	0.58	0.79	0.71
1216 middle				1.33									-24.11										
1216 top	0.67	0.08	0.20	1.77	5.59	0.24	0.65	2.08	8.82	0.48	0.65	0.63	-21.28	1.57	1.01	1.19	1.23	2.35	2.60	0.13	0.99	1.67	0.69
1218 top	0.56	0.24	0.32	1.35	5.66			1.50	9.68	0.44	0.55	0.58	-24.28	<0.7		1.19	0.69	1.29	0.96		0.81	1.45	0.61
1218 middle	0.51	0.31	0.40	0.35	4.84			0.30	8.81	0.33	0.22	0.55	-14.54	<0.8		1.26	0.68	0.61	0.85		0.53	0.80	0.72
1218 base	0.54	0.30	0.37	0.19	4.56			0.20	8.31	0.31	0.14	0.55	-7.85	<0.8		1.20	0.82		1.02		0.53	0.73	0.83
CQ																							
1706b				0.59									14.55										
1709	0.38	0.06	0.10	1.06	5.64			1.30	10.20	0.28	0.66	0.55	12.93	<0.8		1.07	0.73	0.78	0.64		0.72	1.19	0.64
1710	1.07	0.05	0.06	1.02	5.02			1.10	8.29	0.44	0.46	0.61	30.53	<0.8		1.03	0.73	0.97	0.98		0.60	1.02	2.30
1711	0.37	0.05	0.09	0.27	4.81			0.30	8.73	0.16	0.35	0.55	-12.83	<0.8		1.26	0.79	0.46	0.91		0.58	0.86	0.70
1801	0.31	0.08	0.10	0.18	4.47			0.20	8.09	0.15	0.27	0.55	-11.25	<0.9		1.34	0.86		0.95		0.61	0.87	0.65
1802	0.42	0.13	0.10	1.01	5.09			1.20	7.80	0.32	0.61	0.65	17.11	<0.9		1.30	0.91	1.03	0.86		1.12	1.74	0.82

Table A1
(continued)

Sample	Fe-carb	Fe-ox	Fe-mag	FeP	FeT	Inorg-C	TOC	S	Al	$\frac{Fe_{HR}}{FeT}$	$\frac{FeP}{Fe_{HR}}$	$\frac{FeT}{Al}$	$\delta^{34}S$	Mo	U	V	Zn	Pb	Cu	Cd	Ni	Co	Mn
	wt%												permil	Enrichment factor									
CQ																							
1803	0.45	0.12	0.14	0.13	4.68			0.20	8.57	0.18	0.16	0.55	-11.29	<0.8		1.29	0.81	0.36	0.92		0.59	0.93	0.85
1805	0.51	0.09	0.13	1.17	4.79			1.30	8.54	0.39	0.62	0.56	-19.55	<0.8		1.27	0.94	1.77	0.99		0.87	1.42	0.73
1806	0.45	0.06	0.09	1.11	5.26			1.30	8.74	0.32	0.65	0.60	16.57	<0.8		1.15	0.84	0.81	0.79		0.88	1.39	0.83
1807				0.84				1.10					-7.08										
1808	0.61	0.08	0.11	0.91	5.18				8.52	0.33	0.53	0.61	-6.88	<0.8		1.21	0.83	1.10	0.74		0.83	1.48	0.70
1810a	0.38	0.09	0.17	0.88	5.42			1.00	9.63	0.28	0.58	0.56	-14.14	<0.7		1.16	0.71	0.60	0.70		0.68	1.07	0.65
1810c	0.35	0.03	0.04	0.76							0.65		-20.67										
1811	0.53	0.05	0.05	1.01	5.21			1.20	8.14	0.31	0.62	0.64	1.05	<0.84		1.23	0.95	1.04	0.97		0.79	1.32	0.85
1815*				1.23									37.52										
1815	0.52	0.09	0.19	0.89							0.53		12.90										
1902	0.46	0.05	0.12	0.36	4.67			0.40	8.27	0.21	0.36	0.56	-1.45	<0.8		1.25	0.95	0.48	0.93		0.58	0.91	0.85
1903	0.49	0.06	0.12	0.84	5.04			1.00	8.08	0.30	0.55	0.62	10.98	<0.9		1.24	0.91	0.61	0.88		0.70	1.16	0.88
1904	0.47	0.09	0.23	0.83	5.26	0.34	0.31	1.77	8.37	0.31	0.51	0.63	30.77	0.55	1.06	1.18	0.98	0.76	1.18	0.07	0.77	1.20	0.94
1905	0.40	0.04	0.07	0.59	4.80			0.70	8.18	0.23	0.53	0.59	26.16	<0.8		1.23	0.89	0.54	0.92		0.62	0.97	0.85
1906 (1)	0.43	0.07	0.19	0.41	4.76	0.22	0.33	0.60	9.05	0.23	0.37	0.53	15.33	0.42	1.06	1.16	1.22	0.40	1.17	0.09	0.53	0.83	0.82
1906 (2)				0.84									-14.14										
1907 (1)	0.35	0.03	0.08	1.06	5.29			1.30	8.83	0.29	0.70	0.60	-22.69										
1907 (2)				0.83									-18.12										
1908	1.56	0.09	0.06	0.49							0.22		-19.42										
1908 (top)				1.32									-21.98										
BQ																							
2213				0.03																			
2215				0.02																			
2216				0.38									-0.33										
2301				0.98	5.10	0.05	0.31	1.44	8.95			0.57	41.28	0.48	1.07	1.16	1.69	0.66	2.91	0.70	0.72	0.98	0.39
2302				0.43	4.93			0.70	9.23			0.53	-0.73	<0.7		1.14	0.94	1.40	1.50	0.84	0.69	0.91	0.30
2304				0.51	4.37	0.82	0.20	0.78	6.46			0.68	-19.60	0.53	1.15	1.03	2.23	0.95	3.27	0.38	0.97	1.30	2.10
2321	0.63	0.27	0.34	1.39	5.25			1.60	8.32	0.50	0.53	0.63	-18.35	2.47		1.24	0.79	3.74	1.50		1.74	2.02	0.59
2322	0.52	0.15	0.15	1.44	5.17			1.70	8.41	0.44	0.64	0.61	-19.62	2.44		1.16	0.81	3.65	1.50		1.60	2.06	0.67
2323	0.44	0.08	0.04	1.42	5.35	0.18	1.01	1.86	8.76	0.37	0.72	0.61	-20.93	2.48	1.21	1.21	5.10	2.88	2.01	2.08	1.24	1.85	0.63
2324	0.40	0.06	0.04	1.71	5.55	0.30	0.54	2.22	8.68	0.40	0.77	0.64	-20.83	1.42	1.19	1.18	0.97	2.68	1.46	0.12	0.99	1.74	0.74
2325	0.31	0.06	0.09	0.97	5.36			1.10	9.00	0.27	0.68	0.60	-9.96	<0.8		1.22	0.68	0.84	0.79		0.68	1.09	0.71
2326	0.47	0.06	0.09	1.25	5.57			1.40	8.98	0.33	0.67	0.62	28.43	<0.8		1.13	3.44	0.69	1.01	1.73	0.71	1.04	1.10
2327	0.26	0.06	0.02	1.33	5.68	0.25	0.34	1.78	9.39	0.29	0.80	0.60	24.58	0.88	1.00	1.14	0.98	0.84	1.37	0.08	0.68	1.05	0.77

TABLE A1
(continued)

Sample	Fe-carb	Fe-ox	Fe-mag	FeP	FeT	Inorg-C	TOC	S	Al	$\frac{Fe_{HR}}{FeT}$	$\frac{FeP}{Fe_{HR}}$	$\frac{FeT}{Al}$	$\delta^{34}S$	Mo	U	V	Zn	Pb	Cu	Cd	Ni	Co	Mn
	wt%												permil	Enrichment factor									
CQ																							
2328	0.33	0.12	0.11	1.48	5.71			1.70	8.84	0.36	0.73	0.65	8.45	<0.8		1.24	0.74	1.46	0.96		0.80	1.38	0.45
2329	0.24	0.29	0.21	0.48	4.90			0.60	8.71	0.25	0.39	0.56	10.82	<0.8		1.22	0.73	0.71	0.86		0.62	0.97	0.49
2330	0.19	0.08	0.07	0.41	4.66	0.05	0.29	0.55	9.82	0.16	0.55	0.47	15.21	0.36	1.10	1.17	0.86	0.48	1.03	0.02	0.55	0.82	0.43
2331a	0.33	0.08	0.09	0.89	4.97			1.00	8.07	0.28	0.64	0.62	2.88	<0.9		1.19	0.75	1.27	0.95		0.87	1.39	0.72
2332	0.72	0.07	0.08	0.89	5.03	0.69	0.36	1.18	7.80	0.35	0.50	0.64	-17.65	0.80	1.05	1.07	0.98	1.34	1.61	0.06	0.75	1.25	1.54
2333	0.38	0.07	0.08	1.26	5.39	0.25	0.45	1.62	8.87	0.33	0.70	0.61	-13.79	0.83	1.06	1.14	1.10	1.58	1.47	0.04	0.78	1.36	0.81
2334b (i)				1.35	4.52								25.84										
2334b (ii)	0.30	0.08	0.10	0.30		0.33	0.34	0.33	8.60		0.39		-6.96	0.38	1.01	1.11	0.81	0.40	1.42	0.03	0.52	0.75	0.84
2401	0.35	0.04	0.11	1.07	5.23	0.30	0.52	1.38	8.91	0.30	0.68	0.59	-14.80	1.17	1.02	1.16	1.02	1.48	1.57		0.77	1.26	0.79
2402	0.37	0.06	0.15	0.51	4.88			0.50	9.22	0.22	0.47	0.53	-13.20	<0.7		1.07	0.68	0.92	1.09		0.64	0.91	0.84
2403	0.40	0.04	0.08	0.58	5.01	0.35	0.35	0.88	9.02	0.22	0.52	0.56	2.33	0.54	0.99	1.11	1.22	0.79	1.29		0.60	1.00	0.89
2408 base	1.23	0.11	0.08	0.59	4.53					0.44	0.29		-11.62	2.35	1.09	1.15	0.79	3.16	1.88	0.06	1.27	1.90	0.73
2408 top				1.83	5.55	0.24	1.02	2.30	8.85			0.63	-15.55										
2409	0.49	0.11	0.11	0.87							0.55		-8.71										

* Samples from concretions.
YPM[1] Sample from specimen YPM505455, which was collected from the same level as 906.
YPM[2] Sample from specimen YPM506488, which was collected from roughly the same level as bed 1904, except in the Walcott Quarry. See logs for position.

Table A2

Trace element concentrations. Samples were analyzed at SGS labs, with the exception of those in italics, which were analyzed at ACME labs.

	Mo	U	V	Zn	Pb	Cu	Cd	Ni	Co
					PPM				
Detection limits (SGS, *ACME*)	0.05, *2*	0.1, *20*	1, *2*	1, *2*	0.5, *5*	0.5, *2*	0.02, *0.4*	0.5, *2*	0.1, *2*
Walcott Quarry									
822	1.37	4	161	90	13.8	51.7	0.05	39.7	19
902	4.71	4	155	112	49.3	70.9	0.13	71.1	33.8
906	0.88	3.7	151	103	12.8	47.5	0.09	41.1	18.9
YPM[1]	*<2*	*<20*	*149*	*89*	*14*	*33*	*<0.4*	*45*	*21*
912*									
912	1.71	3.9	167	80	21.3	41.9	0.04	45.2	23.9
913	*4*	*<20*	*95*	*223*	*16*	*99*	*0.9*	*32*	*17*
914	*4*	*<20*	*147*	*90*	*35*	*41*	*<0.4*	*66*	*29*
915	3.41	3.5	128	148	42.8	55.6	0.29	57	26.5
916a	1.1	3.9	161	77	20.7	39.3	0.06	43.8	21.8
916b									
916c	*2*	*<20*	*155*	*88*	*44*	*41*	*0.4*	*72*	*33*
916d	*<2*	*<20*	*150*	*88*	*37*	*37*	*<0.4*	*61*	*29*
917	0.83	3	108	121	9.6	98	0.22	36.3	17.6
918	*4*	*<20*	*150*	*85*	*40*	*47*	*<0.4*	*68*	*29*
1001	*6*	*<20*	*128*	*115*	*22*	*57*	*0.5*	*47*	*22*
1002	5.85	3.9	153	114	56.9	102	0.13	177	36.6
1003	1.22	3.5	138	82	15.1	44.9	0.07	43.7	19.7
1004	1.37	3.8	152	107	15.9	50.5	0.09	66.3	22
1004*	3	2.1	116	61.8	14.5	60.5		41.4	33.5
1005	*<2*	*<20*	*157*	*85*	*18*	*33*	*<0.4*	*42*	*18*
1006	*4*	*<20*	*150*	*81*	*18*	*59*	*<0.4*	*50*	*22*
1007	1.18	4	159	78	5.9	46.9	0.06	36	14.1
1008	*2*	*<20*	*108*	*123*	*23*	*50*	*0.4*	*38*	*17*
1008b	*2*	*<20*	*157*	*151*	*37*	*42*	*0.6*	*59*	*27*
1009	2.61	3.1	116	84	26.3	57.9	0.09	44.9	21.2
1010	*6*	*<20*	*143*	*120*	*62*	*74*	*<0.4*	*88*	*34*
1011	*<2*	*<20*	*151*	*73*	*11*	*34*	*<0.4*	*42*	*18*
1012	1.2	3.2	114	160	15.7	225	0.3	35.1	19.5
1013	1.35	3.7	147	89	10.2	53	0.06	49.5	17.9
YPM[2]	*<2*	*<20*	*150*	*82*	*16*	*40*	*<0.4*	*42*	*20*
1101	*2*	*<20*	*152*	*97*	*41*	*48*	*<0.4*	*66*	*31*
1102	3.33	4	152	96	36.7	58.6	0.1	58.9	26.9
1103	*4*	*<20*	*138*	*102*	*46*	*59*	*<0.4*	*72*	*30*
1104	*<2*	*<20*	*101*	*98*	*20*	*69*	*<0.4*	*37*	*18*
1104b	*<2*	*<20*	*86*	*91*	*17*	*79*	*<0.4*	*29*	*15*
1105	*<2*	*<20*	*104*	*82*	*19*	*38*	*<0.4*	*40*	*19*
1106	1.13	2.7	84	641	11.5	621	1.93	29.6	21
1107	1.33	4	161	78	13.8	46.7	0.04	45.6	19.2
1107b	*<2*	*<20*	*159*	*79*	*21*	*45*	*<0.4*	*52*	*22*
1108	*<2*	*<20*	*161*	*76*	*9*	*43*	*<0.4*	*40*	*16*
Tril	1.37	3.7	159	75	12.3	44.4	0.04	43.5	17.4
1203	*<2*	*<20*	*165*	*73*	*14*	*47*	*<0.4*	*48*	*21*
1204	*<2*	*<20*	*159*	*71*	*6*	*42*	*<0.4*	*38*	*13*
1206	*<2*	*<20*	*156*	*71*	*7*	*42*	*<0.4*	*40*	*16*
1210	*<2*	*<20*	*144*	*103*	*36*	*53*	*<0.4*	*57*	*27*
1205	*<2*	*<20*	*159*	*67*	*5*	*36*	*<0.4*	*35*	*13*
1208	1.11	3.8	148	286	8.7	87.6	1.24	36.9	14.4
1211	0.79	3.8	160	100	7.8	57.5	0.07	38.8	14.4
1214	*<2*	*<20*	*154*	*67*	*11*	*38*	*<0.4*	*41*	*18*
1215 base									
1215 middle									
1215c	1.3	3.8	157	96	10.8	63.8	0.02	40.8	15.6
1216 middle									

TABLE A2

(continued)

	Mo	U	V	Zn	Pb	Cu	Cd	Ni	Co
					PPM				
Detection limits (SGS, *ACME*)	0.05, *2*	0.1, *20*	1, *2*	1, *2*	0.5, *5*	0.5, *2*	0.02, *0.4*	0.5, *2*	0.1, *2*
Walcott Quarry									
1216	4.06	3.7	154	116	46.6	116	0.1	67.1	31.4
1218 top	*<2*	*<20*	*168*	*71*	*28*	*47*	*<0.4*	*60*	*30*
1218 middle	*<2*	*<20*	*162*	*64*	*12*	*38*	*<0.4*	*36*	*15*
1218 base	*<2*	*<20*	*146*	*73*	*<5*	*43*	*<0.4*	*34*	*13*
Corner Quarry									
1706b									
1709	*<2*	*<20*	*159*	*80*	*18*	*33*	*<0.4*	*56*	*26*
1710	*<2*	*<20*	*125*	*65*	*18*	*41*	*<0.4*	*38*	*18*
1711	*<2*	*<20*	*161*	*74*	*9*	*40*	*<0.4*	*39*	*16*
1801	*<2*	*<20*	*158*	*74*	*<5*	*39*	*<0.4*	*38*	*15*
1802	*<2*	*<20*	*148*	*76*	*18*	*34*	*<0.4*	*67*	*29*
1803	*<2*	*<20*	*162*	*74*	*7*	*40*	*<0.4*	*39*	*17*
1805	*<2*	*<20*	*159*	*86*	*34*	*43*	*<0.4*	*57*	*26*
1806	*<2*	*<20*	*147*	*78*	*16*	*35*	*<0.4*	*59*	*26*
1807									
1808	*<2*	*<20*	*151*	*76*	*21*	*32*	*<0.4*	*54*	*27*
1810a	*<2*	*<20*	*163*	*73*	*13*	*34*	*<0.4*	*50*	*22*
1810c									
1811	*<2*	*<20*	*146*	*83*	*19*	*40*	*<0.4*	*49*	*23*
1815*									
1815									
1902	*<2*	*<20*	*151*	*84*	*9*	*39*	*<0.4*	*37*	*16*
1903	*<2*	*<20*	*146*	*79*	*11*	*36*	*<0.4*	*43*	*20*
1904	1.35	3.7	145	88	14.3	50	0.05	49.4	21.4
1905	*<2*	*<20*	*147*	*78*	*10*	*38*	*<0.4*	*39*	*17*
1906	1.11	4	154	118	8.1	53.8	0.07	36.5	16
Beecher Quarry									
2301	1.26	4	152	162	13.3	132	0.56	49.3	18.7
2302	*<2*	*<20*	*154*	*93*	*29*	*70*	*0.7*	*49*	*18*
2304	1.01	3.1	97	154	13.8	107	0.22	47.9	17.9
2321	*6*	*<20*	*151*	*70*	*70*	*63*	*<0.4*	*111*	*36*
2322	*6*	*<20*	*143*	*73*	*69*	*64*	*<0.4*	*103*	*37*
2323	6.35	4.4	155	477	56.7	89	1.64	83	34.7
2324	3.61	4.3	150	90	52.4	64.2	0.09	66	32.2
2325	*<2*	*<20*	*161*	*65*	*17*	*36*	*<0.4*	*47*	*21*
2326	*<2*	*<20*	*149*	*330*	*14*	*46*	*1.4*	*49*	*20*
2327	2.42	3.9	156	98	17.8	65	0.07	48.6	21
2328	*<2*	*<20*	*160*	*70*	*29*	*43*	*<0.4*	*54*	*26*
2329	*<2*	*<20*	*156*	*68*	*14*	*38*	*<0.4*	*41*	*18*
2330	1.04	4.5	168	90	10.6	51	0.02	41.5	17.3
2331a	*<2*	*<20*	*141*	*65*	*23*	*39*	*<0.4*	*54*	*24*
2332	1.82	3.4	122	82	23.5	63.4	0.04	44.9	20.8
2333	2.16	3.9	148	104	31.6	65.8	0.03	52.7	25.7
2334	0.96	3.6	140	74	7.7	61.8	0.02	34.1	13.7
2401	3.04	3.8	151	97	29.7	71	<0.02	52.3	23.9
2402	*<2*	*<20*	*144*	*67*	*19*	*51*	*<0.4*	*45*	*18*
2403	1.43	3.7	147	118	16	58.9	<0.02	41.2	19.2
2408	6.07	4	149	75	63	84.3	0.05	86.3	35.9

* = samples from concretions, YPM[1] = sample from specimen YPM505455, which was collected from the same level as 906, YPM[2] = sample from specimen YPM506488, which was collected from roughly the same level as bed 1904, except in the Walcott Quarry. See logs for position.

Table A3

FeD from a subset of samples

Sample	FeD (1hr) wt%	FeD (2hr) wt%
822	0.079	0.092
1005	0.155	0.182
1010	0.177	0.197
1011	0.182	0.205
1013	0.209	0.237
1101	0.147	0.162
1103	0.157	0.176
1104	0.256	0.314
1105	0.201	0.232
1107b	0.169	0.202
1108	0.171	0.203

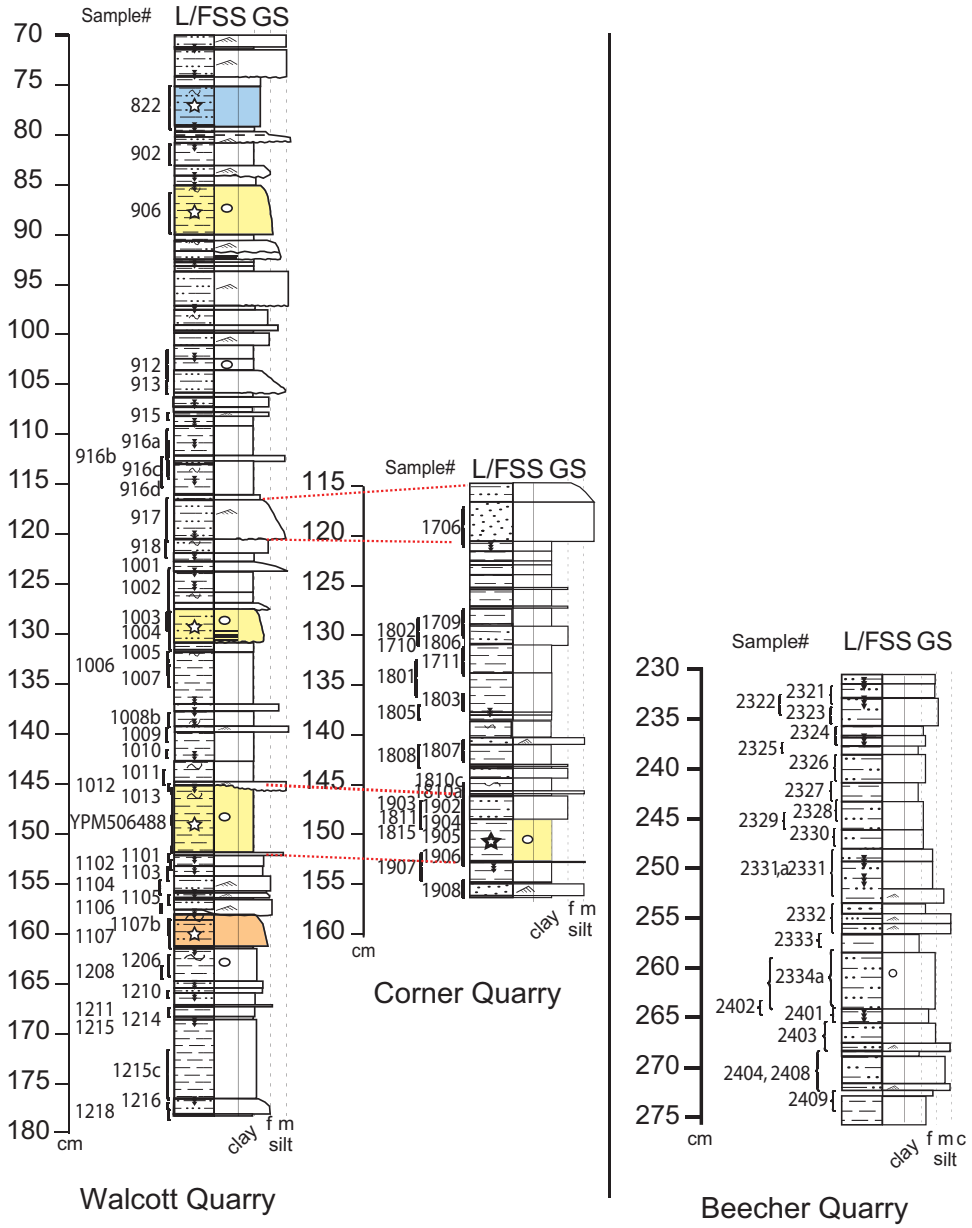

Fig. A1. Walcott, Corner and Beecher Quarry with all sample numbers. Red lines indicate correlated beds. Scale on the left in cm's from marker horizon. See figure 2 for full key.

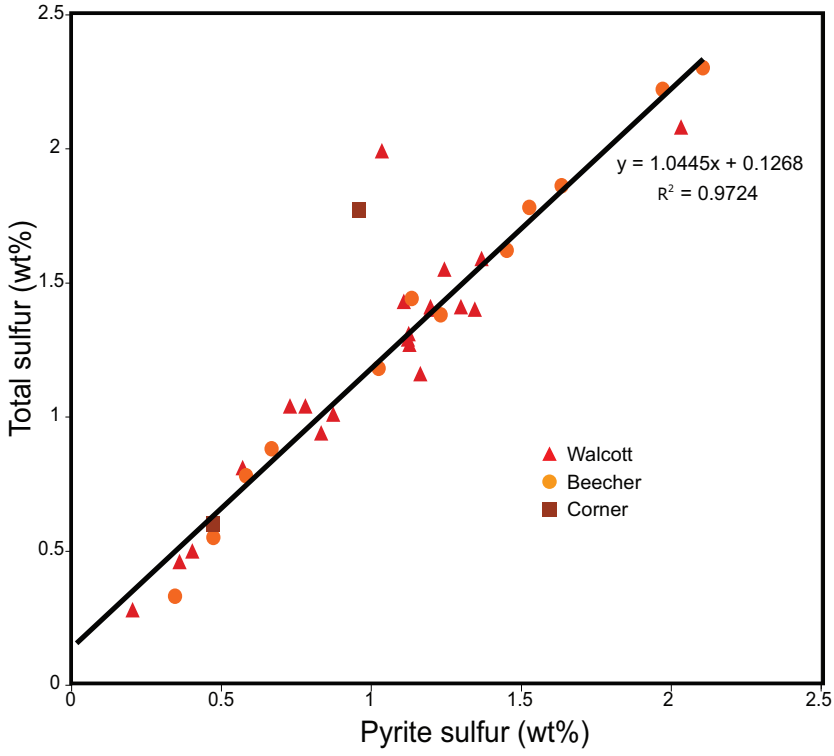

Fig. A2. Total sulfur (wt%) vs. Pyrite sulfur (wt%).

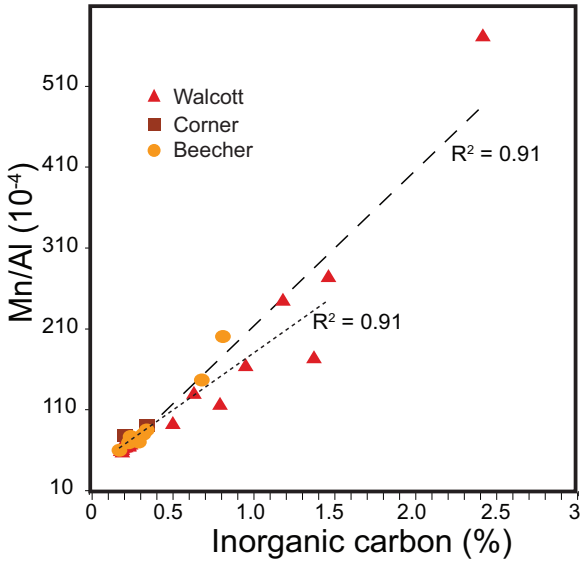

Fig. A3. Mn/Al versus Inorganic carbon (wt%).

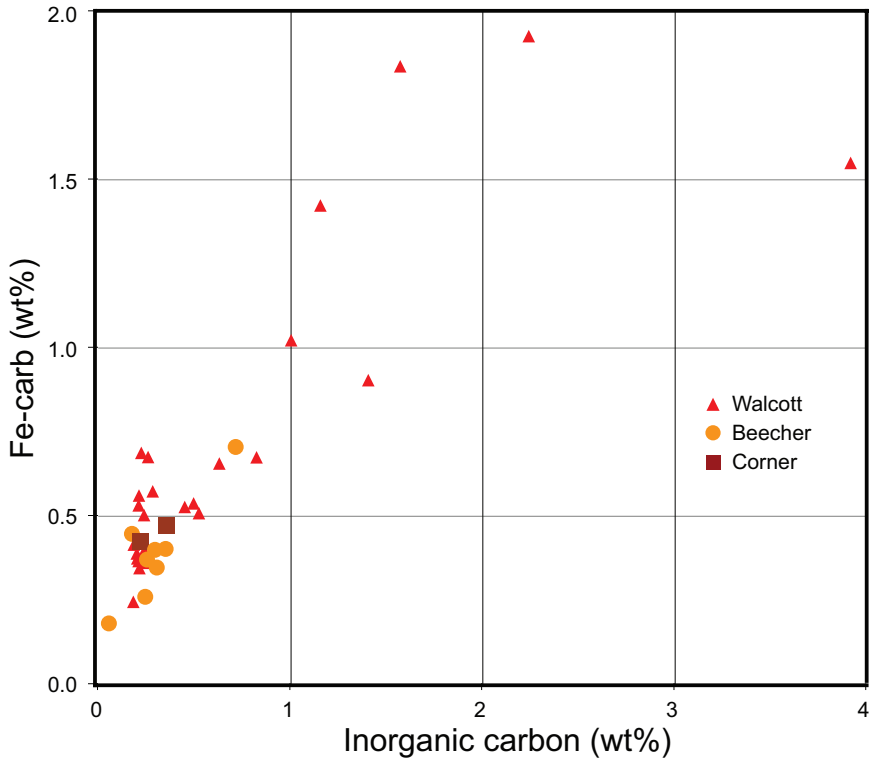

Fig. A4. Fe-carb (wt%) vs. Inorganic carbon (wt%).

References

Algeo, T. J., and Lyons, T. W., 2006, Mo-total organic carbon covariation in modern anoxic marine environments: Implications for analysis of paleoredox and paleohydrographic conditions: Paleoceanography, v. 21, n. 1, p. 1–23, http://dx.doi.org/10.1029/2004PA001112

Algeo, T. J., and Maynard, J. B., 2004, Trace-element behavior and redox facies in core shales of Upper Pennsylvanian Kansas-type cyclothems: Chemical Geology, v. 206, n. 3–4, p. 289–318, http://dx.doi.org/10.1016/j.chemgeo.2003.12.009

——— 2008, Trace-metal covariation as a guide to water-mass conditions in ancient anoxic marine environments: Geosphere, v. 4, n. 5, p. 872–887, http://dx.doi.org/10.1130/GES00174.1

Algeo, T. J., Schwark, L., and Hower, J. C., 2004, High-resolution geochemistry and sequence stratigraphy of the Hushpuckney Shale (Swope Formation, eastern Kansas): implications for climato-environmental dynamics of the Late Pennsylvanian Midcontinent Seaway: Chemical Geology, v. 206, n. 3–4, p. 259–288, http://dx.doi.org/10.1016/j.chemgeo.2003.12.028

Aller, R. C., Madrid, V., Chistoserdov, A., Aller, J. Y., and Heilbrum, C., 2010, Unsteady diagenetic processes and sulfur biogeochemistry in tropical deltaic muds: Implications for oceanic isotope cycles and the sedimentary record: Geochimica et Cosmochimica Acta, v. 74, n. 16, p. 4671–4692, http://dx.doi.org/10.1016/j.gca.2010.05.008

Anderson, T. F., and Raiswell, R., 2004, Sources and mechanisms for the enrichment of highly reactive iron in euxinic black sea sediments: American Journal of Science, v. 304, n. 3, p. 203–233, http://dx.doi.org/10.2475/ajs.304.3.203

Berner, R. A., 1969, Migration of iron and sulfur within anaerobic sediments during early diagenesis: American Journal of Science, v. 267, n. 1, p. 19–42, http://dx.doi.org/10.2475/ajs.267.1.19

Berner, R. A., and Raiswell, R., 1983, Burial of organic carbon and pyrite sulfur in sediments over Phanerozoic time: a new theory: Geochimica et Cosmochimica Acta, v. 47, n. 5, p. 855–862, http://dx.doi.org/10.1016/0016-7037(83)90151-5

Bickert, T., 2006, Influence of geochemical processes on stable isotope distribution in marine sediments, *in* Schulz, H. D., and Zabel, M., editors, Marine Geochemistry: Berlin, Springer, p. 339–369.

Bloch, J., and Krouse, H. R., 1992, Sulfide diagenesis and sedimentation in the Albian Harmon member, Western Canada: Journal of Sedimentary Petrology, v. 62, n. 2, p. 235–249, http://dx.doi.org/10.1306/D42678CF-2B26-11D7-8648000102C1865D

Boyer, D. L., and Droser, M. L., 2009, Palaeoecological patterns within the dysaerobic biofacies: Examples from Devonian black shales of New York state: Palaeogeography, Palaeoclimatology, Palaeoecology, v. 276, n. 1–4, p. 206–216, http://dx.doi.org/10.1016/j.palaeo.2009.03.014

Boyer, D. L., Owens, J. D., Lyons, T. W., and Droser, M. L., 2011, Joining forces: Combined biological and geochemical proxies reveal a complex but refined high-resolution palaeo-oxygen history in Devonian epeiric seas: Palaeogeography, Palaeoclimatology, Palaeoecology, v. 306, n. 3–4, p. 134–146, http://dx.doi.org/10.1016/j.palaeo.2011.04.012

Brett, C. E., Kirchner, B. T., Tsujita, C. J., and Dattilo, B. F., 2008, Depositional dynamics recorded in mixed siliciclastic-carbonate marine successions: Insights from the Upper Ordovician Kope Formation of Ohio and Kentucky, U.S.A: Geological Association of Canada Special Paper, v. 48, p. 73–102.

Briggs, D. E. G., Bottrell, S. H., and Raiswell, R., 1991, Pyritization of soft-bodied fossils: Beecher's Trilobite Bed, Upper Ordovician, New York State: Geology, v. 19, n. 12, p. 1221–1224, http://dx.doi.org/10.1130/0091-7613(1991)019⟨1221:POSBFB⟩2.3.CO;2

Briggs, D. E. G., Raiswell, R., Bottrell, S. H., Hatfield, D., and Bartels, C., 1996, Controls on the pyritization of exceptionally preserved fossils: An analysis of the Lower Devonian Hunsrück Slate of Germany: American Journal of Science, v. 296, n. 6, p. 633–663, http://dx.doi.org/10.2475/ajs.296.6.633

Buck, M. M., ms, 2004, Beecher's Trilobite Bed in the 21st Century: MicroCT analysis of an Ordovician Lagerstätte: Amherst, Massachusetts, Amherst College, Senior thesis, 51 p.

Calvert, S. E., and Pedersen, T. F., 1993, Geochemistry of recent oxic and anoxic marine sediments: Implications for the geological record: Marine Geology, v. 113, n. 1–2, p. 67–88, http://dx.doi.org/10.1016/0025-3227(93)90150-T

——— 1996, Sedimentary geochemistry of manganese: implications for the environment of formation of manganiferous black shales: Economic Geology, v. 91, n. 1, p. 36–47, http://dx.doi.org/10.2113/gsecongeo.91.1.36

Canfield, D. E., 1989, Reactive iron in marine sediments: Geochimica et Cosmochimica Acta, v. 53, n. 3, p. 619–632, http://dx.doi.org/10.1016/0016-7037(89)90005-7

Canfield, D. E., and Berner, R. A., 1987, Dissolution and pyritization of magnetite in anoxic marine sediments: Geochimica et Cosmochimica Acta, v. 51, n. 3, p. 645–639, http://dx.doi.org/10.1016/0016-7037(87)90076-7

Canfield, D. E., and Farquhar, J., 2009, Animal evolution, bioturbation, and the sulfate concentration of the oceans: Proceedings of the National Academy of Sciences of the United States of America, v. 106, n. 20, p. 8123–8127, http://dx.doi.org/10.1073/pnas.0902037106

Canfield, D. E., and Thamdrup, B., 1994, The production of δ^{34}S-depleted sulfide during bacterial disproportionation of elemental sulfur: Science, v. 266, n. 5193, p. 1973–1975, http://dx.doi.org/10.1126/science.11540246

Canfield, D. E., Raiswell, R., Westrich, J. T., Reaves, C. M., and Berner, R. A., 1986, The use of chromium reduction in the analysis of reduced inorganic sulfur in sediments and shales: Chemical Geology, v. 54, n. 1–2, p. 149–155, http://dx.doi.org/10.1016/0009-2541(86)90078-1

Canfield, D. E., Raiswell, R., and Bottrell, S., 1992, The reactivity of sedimentary iron minerals towards sulfide: American Journal of Science, v. 292, n. 9, p. 659–683, http://dx.doi.org/10.2475/ajs.292.9.659

Canfield, D. E., Poulton, S. W., and Narbonne, G. M., 2007, Late-Neoproterozoic deep ocean oxygenation and the rise of animal life: Science, v. 315, n. 5808, p. 92–95, http://dx.doi.org/10.1126/science.1135013

Canfield, D. E., Poulton, S. W., Knoll, A. H., Narbonne, G. M., Ross, G., Goldberg, T., and Strauss, H., 2008, Ferruginous conditions dominated later Neoproterozoic deep-water chemistry: Science, v. 321, n. 5891, p. 949–952, http://dx.doi.org/10.1126/science.1154499

Cisne, J. L., 1973, Beecher's Trilobite Bed revisited: ecology of an Ordovician deepwater fauna: Postilla, v. 160, p. 1–25.

Cisne, J. L., Karig, D. E., Rabe, B. D., and Hay, B. J., 1982, Topography and tectonics of the Taconic outer trench slope as revealed through gradient analysis of fossil assemblages: Lethaia, v. 15, n. 3, p. 229–246, http://dx.doi.org/10.1111/j.1502-3931.1982.tb00647.x

Coleman, M. L., 1985, Geochemistry of diagenetic non-silicate minerals: kinetic considerations: Philosophical Transactions of the Royal Society of London, A, v. 315, p. 39–56, http://dx.doi.org/10.1098/rsta.1985.0028

Cruse, A. M., and Lyons, T. W., 2004, Trace metal records of regional paleoenvironmental variability in Pennsylvanian (Upper Carboniferous) black shales: Chemical Geology, v. 206, n. 3–4, p. 319–345, http://dx.doi.org/10.1016/j.chemgeo.2003.12.010

Crusius, J., Calvert, S., Pedersen, T., and Sage, D., 1996, Rhenium and molybdenum enrichments in sediments as indicators of oxic, suboxic and sulfidic conditions of deposition: Earth and Planetary Science Letters, v. 145, n. 1–4, p. 65–78, http://dx.doi.org/10.1016/S0012-821X(96)00204-X

Curtis, C. D., 1995, Post-depositional evolution of mudstones 1: early days and parental influences: Journal of the Geological Society, London, v. 152, n. 4, p. 577–586, http://dx.doi.org/10.1144/gsjgs.152.4.0577

Dean, W. E., Gardner, J. V., and Piper, D. Z., 1997, Inorganic geochemical indicators of glacial-interglacial changes in productivity and anoxia on the California continental margin: Geochimica et Cosmochimica Acta, v. 61, n. 21, p. 4507–4518, http://dx.doi.org/10.1016/S0016-7037(97)00237-8

Droser, M. L., and Bottjer, D. J., 1993, Trends and patterns of Phanerozoic ichnofabrics: Annual Review of Earth and Planetary Sciences, v. 21, p. 205–225, http://dx.doi.org/10.1146/annurev.ea.21.050193.001225

Farrell, Ú. C., Martin, M. J., Hagadorn, J. W., Whiteley, T., and Briggs, D. E. G., 2009, Beyond Beecher's Trilobite Bed: Widespread pyritization of soft tissues in the Late Ordovician Taconic foreland basin: Geology, v. 37, n. 10 p. 907–910, http://dx.doi.org/10.1130/G30177A.1

Farrell, Ú. C., Briggs, D. E. G., and Gaines, R. R., 2011, Paleoecology of the olenid trilobite *Triarthrus*: New

evidence from Beecher's Trilobite Bed and other sites of pyritization: PALAIOS, v. 26, n. 11, p. 730–742, http://dx.doi.org/10.2110/palo.2011.p11-050r
Fortey, R., 2000, Olenid trilobites: The oldest known chemoautotrophic symbionts: Proceedings of the National Academy of Sciences of the United States of America, v. 97, n. 12, p. 6574–6578, http://dx.doi.org/10.1073/pnas.97.12.6574
Gaines, R. R., and Droser, M. L., 2003, Paleoecology of the familiar trilobite *Elrathia kingii*: An early exaerobic zone inhabitant: Geology, v. 31, n. 11, p. 941–944, http://dx.doi.org/10.1130/G19926.1
Gaines, R. R., Hammarlund, E. U., Hou, X., Qi, C., Gabbott, S. E., Zhao, Y., Peng, J., and Canfield, D. E., 2012, Mechanism for Burgess Shale-type preservation: Proceedings of the National Academy of Sciences of the United States of America, v. 109, n. 14, p. 5180–5184, http://dx.doi.org/10.1073/pnas.1111784109
Gill, B. C., Lyons, T. W., and Saltzman, M. R., 2007, Parallel, high-resolution carbon and sulfur isotope records of the evolving Paleozoic marine sulfur reservoir: Palaeogeography, Palaeoclimatology, Palaeoecology, v. 256, n. 3–4, p. 156–173, http://dx.doi.org/10.1016/j.palaeo.2007.02.030
Gill, B. C., Lyons, T. W., Young, S. A., Kump, L. R., Knoll, A. H., and Saltzman, M. R., 2011, Geochemical evidence for widespread euxinia in the Later Cambrian ocean: Nature v. 469, p. 80–83, http://dx.doi.org/10.1038/nature09700
Goldhaber, M. B., 2003, Sulfur-rich sediments *in* Mackenzie, F. T., Holland, H. D., Turekian, K. K., editors, Treatise on Geochemistry, v. 7: Amsterdam, Elsevier, p. 257–288, http://dx.doi.org/10.1016/B0-08-043751-6/07139-5
Goldhaber, M. B., and Kaplan, I. R., 1980, Mechanisms of sulfur incorporation and isotope fractionation during early diagenesis in sediments of the Gulf of California: Marine Chemistry, v. 9, n. 2, p. 95–143, http://dx.doi.org/10.1016/0304-4203(80)90063-8
Habicht, K. S., and Canfield, D. E., 1997, Sulfur isotope fractionation during bacterial sulfate reduction in organic-rich sediments: Geochimica et Cosmochimica Acta, v. 61, n. 24, p. 5351–5361, http://dx.doi.org/10.1016/S0016-7037(97)00311-6
——— 2001, Isotope fractionation by sulfate-reducing natural populations and the isotopic composition of sulfide in marine sediments: Geology, v. 29, n. 6, p. 555–558, http://dx.doi.org/10.1130/0091-7613(2001)029⟨0555:IFBSRN⟩2.0.CO;2
Hannigan, R. E., and Mitchell, C. E., 1994, The geochemistry of the Utica Shale (Ordovician) of New York State and Quebec, *in* Schultz, A. P., and Rader, E. K., editors, Studies in Eastern Energy and the Environment: AAPG Eastern Section special volume, v. 132, p. 32–37.
Hay, B. J., and Cisne, J. L., 1988, Deposition in the oxygen deficient Taconic Foreland Basin, Late Ordovician *in* Keith, B. D., editor, The Trenton Group (Upper Ordovician Series) of Eastern North America: American Association of Petroleum Geologists, Studies in Geology, v. 29, ch. 8, p. 113–134.
Johnson, D. M., Hooper, P. R., and Conrey, R. M., 1999, XRF analysis of rocks and minerals for major and trace elements on a single low dilution Li-tetraborate fused bead: Advances in X-ray Analysis, v. 41, p. 843–867.
Johnston, D. T., Poulton, S. W., Dehler, C., Porter, S., Husson, J., Canfield, D. E., and Knoll, A. H., 2010, An emerging picture of Neoproterozoic ocean chemistry: insights from the Chuar Group, Grand Canyon, USA: Earth and Planetary Science Letters, v. 290, n. 1–2, p. 64–73, http://dx.doi.org/10.1016/j.epsl.2009.11.059
Johnston, D. T., Poulton, S. W., Goldberg, T., Sergeev, V. N., Podkovyrov, V., Vorob'eva, N. G., Bekker, A., and Knoll, A. H., 2012, Late Ediacaran redox stability and metazoan evolution: Earth and Planetary Science Letters, v. 335–336, p. 25–35, http://dx.doi.org/10.1016/j.epsl.2012.05.010
Jørgensen, B. B., 1979, A theoretical model of the stable sulfur isotope distribution in marine sediments: Geochimica et Cosmochimica Acta, v. 43, n. 3, p. 363–374, http://dx.doi.org/10.1016/0016-7037(79)90201-1
Kampschulte, A., and Strauss, H., 2004, The sulfur isotopic evolution of Phanerozoic seawater based on the analysis of structurally substituted sulfate in carbonates: Chemical Geology, v. 204, n. 3–4, p. 255–286, http://dx.doi.org/10.1016/j.chemgeo.2003.11.013
Kasten, S., Freundenthal, T., Gingele, F. X., and Schulz, H. D., 1998, Simultaneous formation of iron-rich layers at different redox boundaries in sediments of the Amazon deep-sea fan: Geochimica et Cosmochimica Acta, v. 62, n. 13, p. 2253–2264, http://dx.doi.org/10.1016/S0016-7037(98)00093-3
Lehmann, D., Brett, C. E., Cole, R., and Baird, G., 1995, Distal sedimentation in a peripheral foreland basin: Ordovician black shales and associated flysch of the western Taconic foreland, New York State and Ontario: Geological Society of America Bulletin, v. 107, n. 6, p. 708–724, http://dx.doi.org/10.1130/0016-7606(1995)107⟨0708:DSIAPF⟩2.3.CO;2
Levin, L. A., 2003, Oxygen minimum zone benthos: adaptation and community response to hypoxia: Oceanography and Marine Biology: an Annual Review, v. 41, p. 1–45.
Levin, L. A., Gage, J. D., Martin, C., and Lamont, P. A., 2000, Macrobenthic community structure within and beneath the oxygen minimum zone, NW Arabian Sea: Deep-Sea Research Part II: Topical Studies in Oceanography, v. 47, n. 1–2, p. 189–226, http://dx.doi.org/10.1016/S0967-0645(99)00103-4
Lyons, T. W., 1997, Sulfur isotopic trends and pathways of iron sulfide formation in upper Holocene sediments of anoxic Black Sea: Geochimica et Cosmochimica Acta, v. 61, n. 16, p. 3367–3382, http://dx.doi.org/10.1016/S0016-7037(97)00174-9
Lyons, T. W., and Severmann, S., 2006, A critical look at iron paleoredox proxies: New insights from modern euxinic marine basins: Geochimica et Cosmochimica Acta, v. 70, n. 23, p. 5698–5722, http://dx.doi.org/10.1016/j.gca.2006.08.021
Lyons, T. W., Werne, J. P., Hollander, D. J., and Murray, R. W., 2003, Contrasting sulfur geochemistry and Fe/Al and Mo/Al ratios across the last oxic-to-anoxic transition in the Cariaco Basin, Venezuela: Chemical Geology, v. 195, n. 1–4, p. 131–157, http://dx.doi.org/10.1016/S0009-2541(02)00392-3
Lyons, T. W., Anbar, A. D., Severmann, S., Scott, C., and Gill, B. C., 2009, Tracking euxinia in the ancient

ocean: a multiproxy perspective and Proterozoic case study: Annual Review of Earth and Planetary Sciences, v. 37, p. 507–534, http://dx.doi.org/10.1146/annurev.earth.36.031207.124233
Macquaker, J. H. S., Curtis, C. D., and Coleman, M. L., 1997, The role of iron in mudstone diagenesis: comparison of Kimmeridge Clay formation mudstones from onshore and offshore (UKCS) localities: Journal of Sedimentary Research, v. 67, p. 871–878, http://dx.doi.org/10.1306/D426865D-2B26-11D7-8648000102C1865D
März, C., Poulton, S. W., Beckmann, B., Kuster, K., Wagner, T., and Kasten, S., 2008, Redox sensitivity of P cycling during marine black shale formation: Dynamics of sulfidic and anoxic, non-sulfidic bottom waters: Geochimica et Cosmochimica Acta, v. 72, n. 15, p. 3703–3717, http://dx.doi.org/10.1016/j.gca.2008.04.025
Mucci, A., and Edenborn, H. M., 1992, Influence of an organic-poor landslide deposit on the early diagenesis of iron and manganese in a coastal marine sediment: Geochimica et Cosmochimica Acta, v. 56, n. 11, p. 3909–3921, http://dx.doi.org/10.1016/0016-7037(92)90005-4
Poulton, S. W., and Canfield, D. E., 2005, Development of a sequential extraction procedure for iron: implications for iron partitioning in continentally derived particulates: Chemical Geology, v. 214, n. 3–4, p. 209–221, http://dx.doi.org/10.1016/j.chemgeo.2004.09.003
——— 2011, Ferruginous conditions: A dominant feature of the ocean through Earth's history: Elements, v. 7, n. 2, p. 107–112, http://dx.doi.org/10.2113/gselements.7.2.107
Poulton, S. W., Fralick, P. W., and Canfield, D. E., 2004, The transition to a sulfidic ocean ~1.84 billion years ago: Nature, v. 431, p. 173–177, http://dx.doi.org/10.1038/nature02912
Poulton, S. W., and Raiswell, R., 2002, The low-temperature geochemical cycle of iron: from continental fluxes to marine sediment deposition: American Journal of Science, v. 302, n. 9, p. 774–805, http://dx.doi.org/10.2475/ajs.302.9.774
Pujol, F., Berner, Z., and Stüben, D., 2006, Palaeoenvironmental changes at the Frasnian/Famennian boundary in key European sections: Chemostratigraphic constraints: Palaeogeography, Palaeoclimatology, Palaeoecology, v. 240, n. 1–2, p. 120–145, http://dx.doi.org/10.1016/j.palaeo.2006.03.055
Raiswell, R., 1988, Evidence for surface reaction-controlled growth of carbonate concretions in shales: Sedimentology, v. 35, n. 4, p. 571–575, http://dx.doi.org/10.1111/j.1365-3091.1988.tb01236.x
——— 1997, A geochemical framework for the application of stable sulphur isotopes to fossil pyritization: Journal of the Geological Society, London, v. 154, n. 2, p. 343–356, http://dx.doi.org/10.1144/gsjgs.154.2.0343
Raiswell, R., and Berner, R. A., 1986, Pyrite and organic matter in Phanerozoic normal marine shales: Geochimica et Cosmochimica Acta, v. 50, n. 9, p. 1967–1976, http://dx.doi.org/10.1016/0016-7037(86)90252-8
Raiswell, R., and Canfield, D. E., 1998, Sources of iron for pyrite formation in marine sediments: American Journal of Science, v. 298, n. 3, p. 219–245, http://dx.doi.org/10.2475/ajs.298.3.219
Raiswell, R., Canfield, D. E., and Berner, R. A., 1994, A comparison of iron extraction methods for the determination of degree of pyritisation and the recognition of iron-limited pyrite formation: Chemical Geology, v. 111, n. 1–4, p. 101–110, http://dx.doi.org/10.1016/0009-2541(94)90084-1
Raiswell, R., Newton, R. J., and Wignall, P. B., 2001, An indicator of water-column anoxia: resolution of biofacies variations in the Kimmeridge Clay (Upper Jurassic, U.K.): Journal of Sedimentary Research, v. 71, n. 2, p. 286–294, http://dx.doi.org/10.1306/070300710286
Raiswell, R., Newton, R., Bottrell, S. H., Coburn, P. M., Briggs, D. E. G., Bond, D. P., and Poulton, S. W., 2008, Turbidite depositional influences on the diagenesis of Beecher's Trilobite Bed and the Hunsrück Slate; sites of soft tissue pyritization: American Journal of Science, v. 308, n. 2, p. 105–129, http://dx.doi.org/10.2475/02.2008.01
Raiswell, R., Reinhard, C. T., Derkowski, A., Owens, J., Bottrell, S. H., Anbar, A. D., and Lyons, T. W., 2011, Formation of syngenetic and early diagenetic iron minerals in the late Archaen Mt. McRae Shale, Hamersley Basin, Australia: New insights on the patterns, controls and paleoenvironmental implications of authigenic mineral formation: Geochimica et Cosmochimica Acta, v. 75, n. 4, p. 1072–1087, http://dx.doi.org/10.1016/j.gca.2010.11.013
Rice, C. A., Tuttle, M. L., and Reynolds, R. L., 1993, The analysis of forms of sulfur in ancient sediments and sedimentary rocks: comments and cautions: Chemical Geology, v. 107, n. 1–2, p. 83–95, http://dx.doi.org/10.1016/0009-2541(93)90103-P
Ross, D. J. K., and Bustin, R. M., 2009, Investigating the use of sedimentary geochemical proxies for paleoenvironment interpretation of thermally mature organic-rich strata: examples from the Devonian-Mississippian shales, Western Canadian sedimentary basin: Chemical Geology, v. 260, n. 1–2, p. 1–19, http://dx.doi.org/10.1016/j.chemgeo.2008.10.027
Sageman, B. B., and Lyons, T. W., 2003, Geochemistry of fine-grained sediments and sedimentary rocks, *in* Mackenzie, F. T., Holland, H. D., Turekian, K. K., editors, Treatise on Geochemistry, v. 7, Sediments, Diagenesis, and Sedimentary Rocks: Amsterdam, Elsevier, p. 115–158, http://dx.doi.org/10.1016/B0-08-043751-6/07157-7
Savrda, C. E., and Bottjer, D. J., 1991, Oxygen-related biofacies in marine strata: An overview and update: Geological Society, London, Special Publications, v. 58, p. 201–219, http://dx.doi.org/10.1144/GSL.SP.1991.058.01.14
Thompson, J. B., Mullins, H. T., Newton, C. R., and Vercoutere, T. L., 1985, Alternative biofacies model for dysaerobic communities: Lethaia, v. 18, n. 2, p. 167–179, http://dx.doi.org/10.1111/j.1502-3931.1985.tb00695.x
Tribovillard, N., Algeo, T. J., Lyons, T., and Riboulleau, A., 2006, Trace metals as paleoredox and paleoproductivity proxies: An update: Chemical Geology, v. 232, n. 1–2, p. 12–32, http://dx.doi.org/10.1016/j.chemgeo.2006.02.012
Turekian, K. K., and Wedepohl, K. H., 1961, Distribution of the elements in some major units of the earth's

crust: Geological Society of America Bulletin, v. 72, n. 2, p. 175–192, http://dx.doi.org/10.1130/0016-7606(1961)72[175:DOTEIS]2.0.CO;2

Turgeon, S., and Brumsack, H.-J., 2006, Anoxic vs. dysoxic events reflected in sediment geochemistry during the Cenomanian-Turonian Boundary Event (Cretaceous) in the Umbria-Marche Basin of central Italy: Chemical Geology, v. 234, n. 3–4, p. 321–339, http://dx.doi.org/10.1016/j.chemgeo.2006.05.008

Tyson, R. V., and Pearson, T. H., 1991, Modern and ancient continental shelf anoxia: an overview: Geological Society, London, Special Publications, v. 58, p. 1–24, http://dx.doi.org/10.1144/GSL.SP.1991.058.01.01

Warren, J., 2000, Dolomite: occurrence, evolution and economically important associations: Earth Science Reviews, v. 52, n. 1–3, p. 1–81, http://dx.doi.org/10.1016/S0012-8252(00)00022-2

Wedepohl, K. H., 1971, Environmental influences on the chemical composition of shales and clays: Physics and Chemistry of the Earth, v. 8, p. 305–333, http://dx.doi.org/10.1016/0079-1946(71)90020-6

Werne, J. P., Sageman, B. B., Lyons, T. W., and Hollander, D. J., 2002, An integrated assessment of a "type euxinic" deposit: Evidence for multiple controls on black shale deposition in the Middle Devonian Oatka Creek Formation: American Journal of Science, v. 302, n. 2, p. 110–143, http://dx.doi.org/10.2475/ajs.302.2.110

Whittington, H. B., and Almond, J. E., 1987, Appendages and habits of the Upper Ordovician trilobite *Triarthrus eatoni*: Philosophical Transactions of the Royal Society of London, B, v. 317, n. 1182, p. 1–46, http://dx.doi.org/10.1098/rstb.1987.0046

Wignall, P. B., 1993, Distinguishing between oxygen and substrate control in fossil benthic assemblages: Journal of the Geological Society, London, v. 150, n. 1, p. 193–196, http://dx.doi.org/10.1144/gsjgs.150.1.0193

——— 1994, Black Shales: Oxford, Oxford University Press, 144 p.

Wilson, T. R. S., Thomson, J., Hydes, D. J., Colley, S., Culkin, F., and Sørensen, J., 1986, Oxidation fronts in pelagic sediments: Diagenetic formation of metal-rich layers: Science, v. 232, n. 4753, p. 972–975, http://dx.doi.org/10.1126/science.232.4753.972

Xu, G., Hannah, J. L., Bingen, B, Georgiev, S., and Stein, H. J., 2012b, Digestion methods for trace element measurements in shales: Paleoredox proxies examined: Chemical Geology, v. 324–325, p. 132–147, http://dx.doi.org/10.1016/j.chemgeo.2012.01.029

Xu, L., Lehmann, B., Mao, J., Nägler, T., F., Neubert, N., Böttcher, M., E., and Escher, P., 2012a, Mo isotope and trace element patters of Lower Cambrian black shales in China: Multi-proxy constraints on paleoenvironment: Chemical Geology, v. 318–319, p. 45–59, http://dx.doi.org/10.1016/j.chemgeo.2012.05.016

Yudina, A. B., Racki, G., Savage, N. M., Racka, M., and Małkowski, K., 2002, The Frasnian-Famennian events in a deep-shelf succession, Subpolar Urals: Biotic, depositional, and geochemical records: Acta Palaeontologica Polonica, v. 47, n. 2, p. 355–372.

Zhabina, N. N., and Volkov, I. I., 1978, A method of determination of various sulfur compounds in sea sediments and rocks, *in* Krumbein, W. E., editor, Environmental Biogeochemistry and Geomicrobiology, Methods, Metals and Assessment 3: Ann Arbor, Ann Arbor Science Publishers, p. 735–746.